PURPOSE-LED PUBLISHING™

TOPICAL REVIEW

A review on magnetic and spintronic neurostimulation: challenges and prospects

To cite this article: Renata Saha *et al* 2022 *Nanotechnology* **33** 182004

IOP Publishing Nanotechnology
Nanotechnology 33 (2022) 182004 (34pp) https://doi.org/10.1088/1361-6528/ac49be

Topical Review

A review on magnetic and spintronic neurostimulation: challenges and prospects

Renata Saha[1,*], Kai Wu[1], Robert P Bloom[1], Shuang Liang[2], Denis Tonini[1] and Jian-Ping Wang[1,*]

[1] Department of Electrical and Computer Engineering, University of Minnesota, Minneapolis, MN 55455, United States of America
[2] Department of Chemical Engineering and Material Science, University of Minnesota, Minneapolis, MN 55455, United States of America

E-mail: saha0072@umn.edu and jpwang@umn.edu

Received 9 September 2021, revised 6 December 2021
Accepted for publication 10 January 2022
Published 10 February 2022

Abstract

In the treatment of neurodegenerative, sensory and cardiovascular diseases, electrical probes and arrays have shown quite a promising success rate. However, despite the outstanding clinical outcomes, their operation is significantly hindered by non-selective control of electric fields. A promising alternative is micromagnetic stimulation (μMS) due to the high permeability of magnetic field through biological tissues. The induced electric field from the time-varying magnetic field generated by magnetic neurostimulators is used to remotely stimulate neighboring neurons. Due to the spatial asymmetry of the induced electric field, high spatial selectivity of neurostimulation has been realized. Herein, some popular choices of magnetic neurostimulators such as microcoils (μcoils) and spintronic nanodevices are reviewed. The neurostimulator features such as power consumption and resolution (aiming at cellular level) are discussed. In addition, the chronic stability and biocompatibility of these implantable neurostimulator are commented in favor of further translation to clinical settings. Furthermore, magnetic nanoparticles (MNPs), as another invaluable neurostimulation material, has emerged in recent years. Thus, in this review we have also included MNPs as a remote neurostimulation solution that overcomes physical limitations of invasive implants. Overall, this review provides peers with the recent development of ultra-low power, cellular-level, spatially selective magnetic neurostimulators of dimensions within micro- to nano-range for treating chronic neurological disorders. At the end of this review, some potential applications of next generation neuro-devices have also been discussed.

Keywords: neurostimulation, micromagnetic stimulation, microcoils, spintronic nanodevices, magnetic nanoparticle, spatially selective, ultra-low power

(Some figures may appear in colour only in the online journal)

1. Introduction

The stimulation of excitable tissues using electrical probes and arrays have a long history. For instance, for the treatment of Parkinson's disease, epilepsy, dystonia, tremor and obsessive compulsive disorder (OCD), deep brain stimulation (DBS) implants have proved to be quite successful [1] (see figure 1(a)). Besides, cardiac pacemakers [2], cochlear implants [3], limb [4] and retinal [5] prostheses have shown an exceptional success rate. However, these electrical implants suffer from several technical and biological set-backs. From a technical point of view, conductive DBS leads

* Authors to whom any correspondence should be addressed.

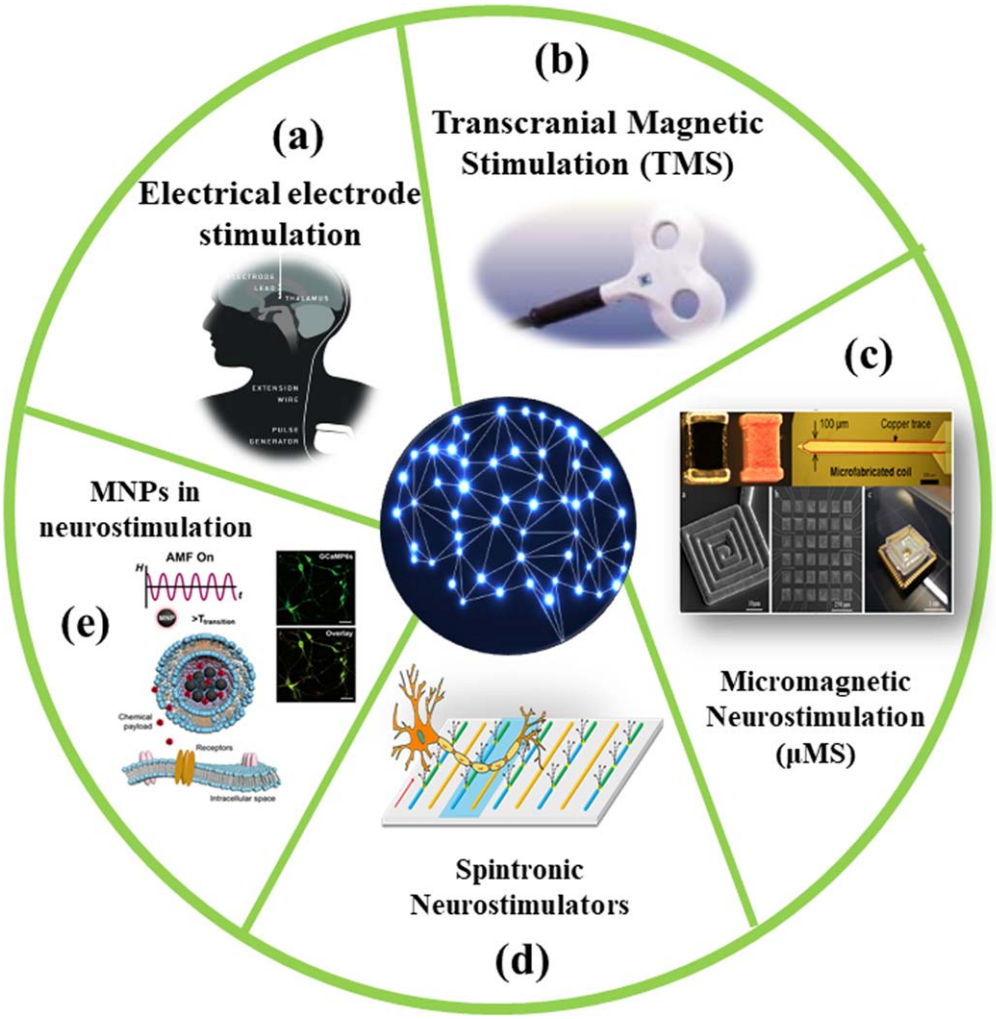

Figure 1. Neurostimulation techniques which inspired in this review work. (a) Electrical electrode-based stimulation which is clinically termed as deep brain stimulation (DBS). Reproduced with permission from [11]. There have been many interesting review works based out of this technology in terms of clinical trials, electrode development etc [1, 12, 13]. (b) Transcranial magnetic stimulation (TMS). Reprinted by permission from Springer Nature Customer Service Centre GmbH: Springer Nature, Nature Reviews Neuroscience, [14], Copyright © 2000, Macmillan Magazines Ltd. DBS is a Food and Drug Administration (FDA)-approved treatment for epilepsy and TMS is FDA-approved for treatment of major depression. Magnetic neurostimulation strategies: both (a) and (b) has inspired towards the development of (c) micromagnetic neurostimulation (μMS). Reprinted by permission from Springer Nature Customer Service Centre GmbH: Springer Nature, Nature Communications, [15–17], Copyright © 2012, The Author(s) and (d) Spintronic neurostimulators. Reprinted from [18], with the permission of AIP Publishing. Both (c) and (d) are neural implants. (e) Magnetic nanoparticles (MNPs) externally manipulated by alternating-gradient magnetic field (AMF) for focal, non-invasive neurostimulation. Reprinted by permission from Springer Nature Customer Service Centre GmbH: Springer Nature, Nature Nanotechnology, [19], Copyright © 2019, The Author(s), under exclusive licence to Springer Nature Limited.

interact with the radio frequency (RF) waves during an MRI test which induces currents within the leads. This generates heat energy that causes detrimental thermal effects on neighboring tissues and renders DBS electrodes highly MRI incompatible [6, 7]. This nuance of DBS implants has been coined as the 'antenna effect' [8]. As these implants are in galvanic contact with tissues, they cause biofouling, leading to glial cell scarring, tissue inflammation and immune reaction [9, 10]. This eventually causes the electrical leads to operate at significantly higher thresholds than necessary, often demanding replacement with new DBS leads through a painful and expensive surgical procedure. Transcranial magnetic stimulation (TMS, figure 1(b)) has the advantage of being non-invasive, but is not very spatially selective, and it does not penetrate deep into the brain because magnetic fields decay over the distance cubed, unlike electrical signals, which decay over the distance squared. Therefore, TMS cannot stimulate structures located deep in the brain, which are targets of neurological disorders such as Parkinson's disease and essential tremor.

Micromagnetic stimulation (μMS) becomes a promising alternative to the electrodes. Some micromagnetic devices/arrays such as microcoils (μcoils, figure 1(c)) and spintronic nanodevices (figure 1(d)) may be able to stimulate with much larger amplitudes and tissue volumes than the same sized electrodes. Stimulation with magnetic fields does not require an electrochemical interface and therefore can be scaled down in size to achieve high spatial precision. There has also been a

pathbreaking discovery in the near past through magnetic stimulation of neurons by *in vivo* delivery of magnetic nanoparticles (MNPs) externally controlled by high intensity alternating magnetic field (AMF) gradient [20] (see figure 1(e)). Relying on the remote control of magnetic fields, the MNPs and magnetic nanodiscs can trigger temperature-, mechano-, and/or voltage-sensitive ion channels and eventually cause activation of nearby neurons. This effect when integrated with chemogenetic activation of engineered receptors, permits control of specific neurons at a spatial and temporal precision [19, 21].

Figure 1 summarizes different magnetic neurostimulators of interest discussed in this review and table 2, in section 6 systematically compares their performances. This paper is arranged as follows: fundamentals of neurostimulation are outlined in section 2, micromagnetic neurostimulation (μMS) is reviewed in section 3, spintronic nanodevices and MNPs as neurostimulators are reviewed in sections 4 and 5, respectively. Challenges and opportunities of magnetic neurostimulation are discussed in section 6 which is followed by concluding remarks in section 7.

2. Fundamentals of neurostimulation

2.1. Strength, duration and frequency of stimulus

Neurostimulation or firing of neurons involves a unique combination of chemical → electrical → chemical → phenomena. However, to artificially fire the neurons, a stimulus of a certain combination of strength and duration needs to be applied. The minimum current of infinite duration required to bring the neurons to threshold is the rheobase, while the minimum duration to fire the neurons at twice the strength of rheobase is termed as the chronaxie (see figure 2(a)). The idea is to select the correct combination of strength–duration values such that they lie on the strength–duration curve (black-colored line in figure 2(a)). Very recently, a third parameter has been proposed to be extremely important for neurostimulation: the frequency at which the stimulus is applied. Repetitive electrical stimulation can activate neurons even when the strength of the stimuli are significantly lower than the threshold [22]. For instance, Chan and Nicholson's reports in 1986 [23] showed that for the firing of hippocampal neurons, the threshold field strength is required to be a single pulse of 10 V m^{-1} amplitude. But in 2003, Francis *et al*'s work [24] reported that an electric field strength of only 0.14 V m^{-1} is sufficient to stimulate hippocampal neurons provided the stimuli is delivered within a frequency range of 1–2 Hz. The concept of repetitive magnetic stimulation (r-MS) is undoubtedly encouraging, as this signifies lower threshold of neurostimulation, implying reduced neuron damage.

2.2. Molecular events behind neuron firing: action potential

The building blocks of the nervous system are the neurons which consist of three main parts: cell body (or soma), axon and axon terminal (see figure 2(b)). Figure 2(c) the basic cross-section of a neuron membrane composed of ion channels, ions, and proteins. In neurons, between the intracellular (represented by yellow background in figure 2(c)) and extracellular fluids (represented by blue background in figure 2(c)), there is a difference in ionic potential due to the concentration differences of ions such as Na^+, K^+, Cl^- and Ca^{2+} (see figure 2(c)). This causes an electric potential difference that is modeled by the Nernst Equation [27]:

$$E_{ion} = -\frac{RT}{zF_c}\log\left(\frac{C_{\text{out}}}{C_{\text{in}}}\right), \tag{1}$$

where, E_{ion} is the cell potential (in mV), R is the universal gas constant (8.314 472 J K^{-1} mol^{-1}), T is the temperature (in K), z is the valency of the ion, F_c is the Faraday's constant (9.648 533 99(24) × 10^4 C mol^{-1}), C_{out} and C_{in} are the total concentrations of all the ions moving in and out of the extracellular membrane, respectively (see figure 2(c)). The study of ionic conduction through neuron membranes and elicitation of action potential were pioneered before 1955 by Hodgkin and Huxley who along with J. C. Eccles were awarded the Nobel Prize in Physiology or Medicine in 1963 [28]. Connection between two neurons is also built in this process, where the neurotransmitters accumulated in synaptic vesicles from one neuron (represented in blue in figure 2(d), neuron 1) are transmitted through the synaptic cleft to the receptors on ion channels in the adjacent neuron (represented in pink in figure 2(d), neuron 2). This forms the synapse between two neighboring neurons where the axon terminal of one connects to the dendrites of the other neuron.

When the neurons are at equilibrium, this potential is at −65 mV termed as the resting membrane potential (see step 1 in figure 3(a)). In response to an electrical, chemical, mechanical, thermal or optical stimulus, specific voltage-sensitive (electrical stimulus), ligand-gated (chemical stimulus), mechanically-gated (mechanical stimulus), temperature-gated (thermal stimulus), or light-gated (optical stimulus) ion channels are opened (see figure 3(b)) and ions influx/outflux the cell membranes along concentration gradients [29]. Due to an influx of Na^+ ions in the neurons and outflux of K^+ ions from the neurons, the electric potential increases (depolarization, see step 2 in figure 3(a)). At this stage the cell potential reaches a peak at +45 mV (see step 3 in figure 3(a)). This is followed by repolarization (see step 4 in figure 3(a)), a phenomenon that involves outflux of Na^+ ions from the neurons and influx of K^+ ions inside the neurons. During repolarization, the cell potential starts to fall to a negative value. It reaches a value of −70 mV when the cell is said to be in refractory period or undershoot period (see step 5 in figure 3(a)). This brief refractory period is the separation between two consecutive action potentials. This cycle of molecular events, from step 1 through 5 in figure 3(a), concerning the transition from resting membrane potential to refractory period or undershoot, is termed as the action potential.

2.3. Recording neuronal responses

Neuron responses can be measured *in vitro* as well as *in vivo*. *In vivo* recordings require implantation of recording electrodes in the brain or spinal cords of animals. Special

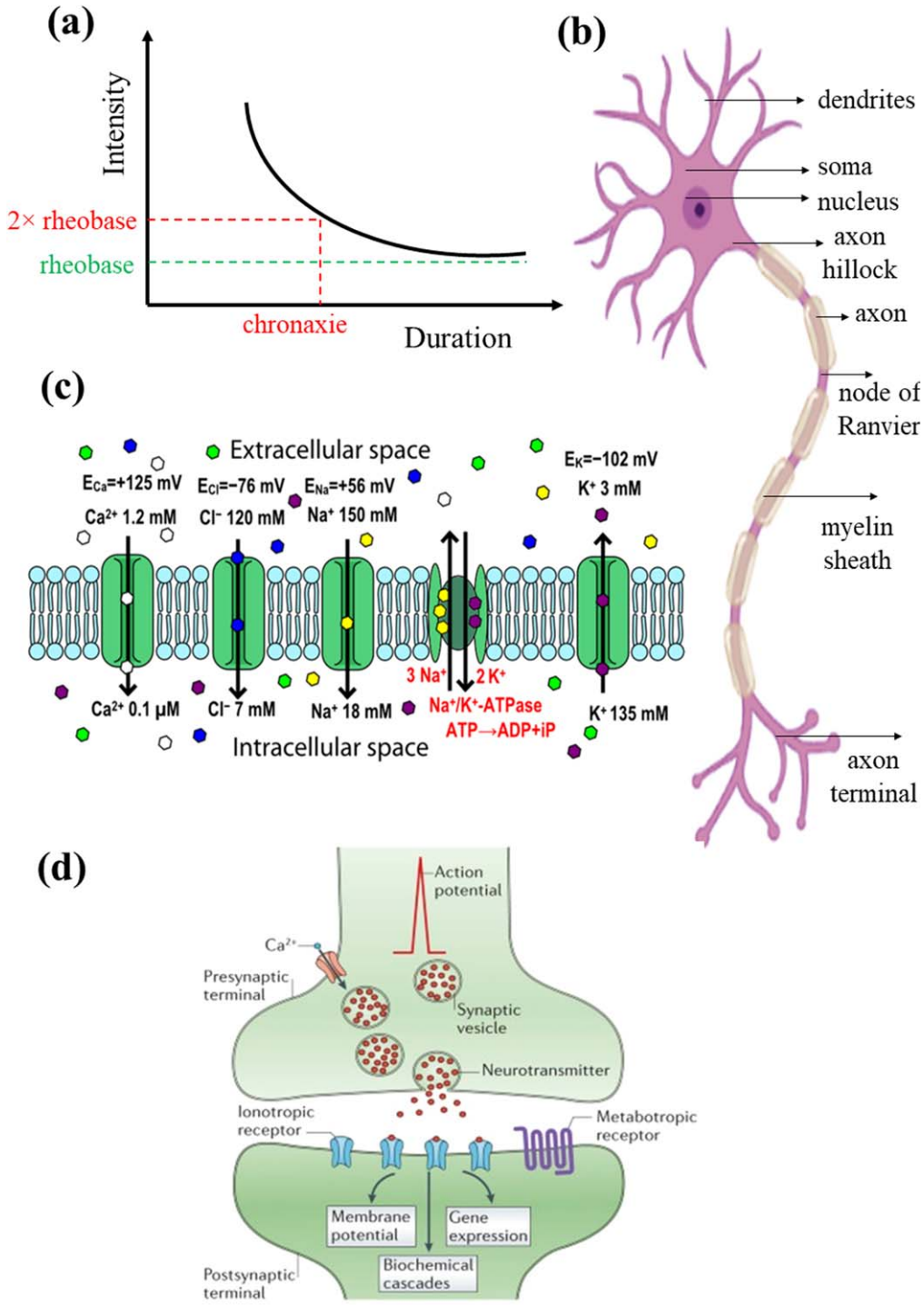

Figure 2. (a) Schematic of the strength–duration curve for neurostimulation. (b) Schematic demonstration of different parts of a neuron. (c) Basic illustration of a neuron membrane. Reproduced from [25]. CC BY 4.0. (d) The components of the synaptic cleft that forms the connection between two neurons. Reprinted by permission from Springer Nature Customer Service Centre GmbH: Springer Nature, Nature Reviews Neuroscience, [26], Copyright © 2014, Nature Publishing Group, a division of Macmillan Publishers Limited. All Rights Reserved.

mention includes, Michigan arrays [31] (see figure 4(a)), the 3D Utah arrays [32] (see figure 4(b)), both of which are implantable and invasive neural recording strategies. Some non-invasive recording and/or imaging approaches include electroencephalogram (EEG) (see figure 4(c)), magnetoencephalogram (MEG, see figure 4(d)), computed tomography scan (CT scan), magnetic resonance imaging (MRI, see figure 4(e)), etc. *In vitro* recordings require preparation of the neuron tissue slice in an electrolytic solution and observation of the responses using patch-clamp or recording the local field potential (LFP) using glass micropipette micromanipulator (see figure 4(f)). Other popular methods for *in vitro* recording of neural responses include Ca-fluorescence imaging [33–35], flavoprotein

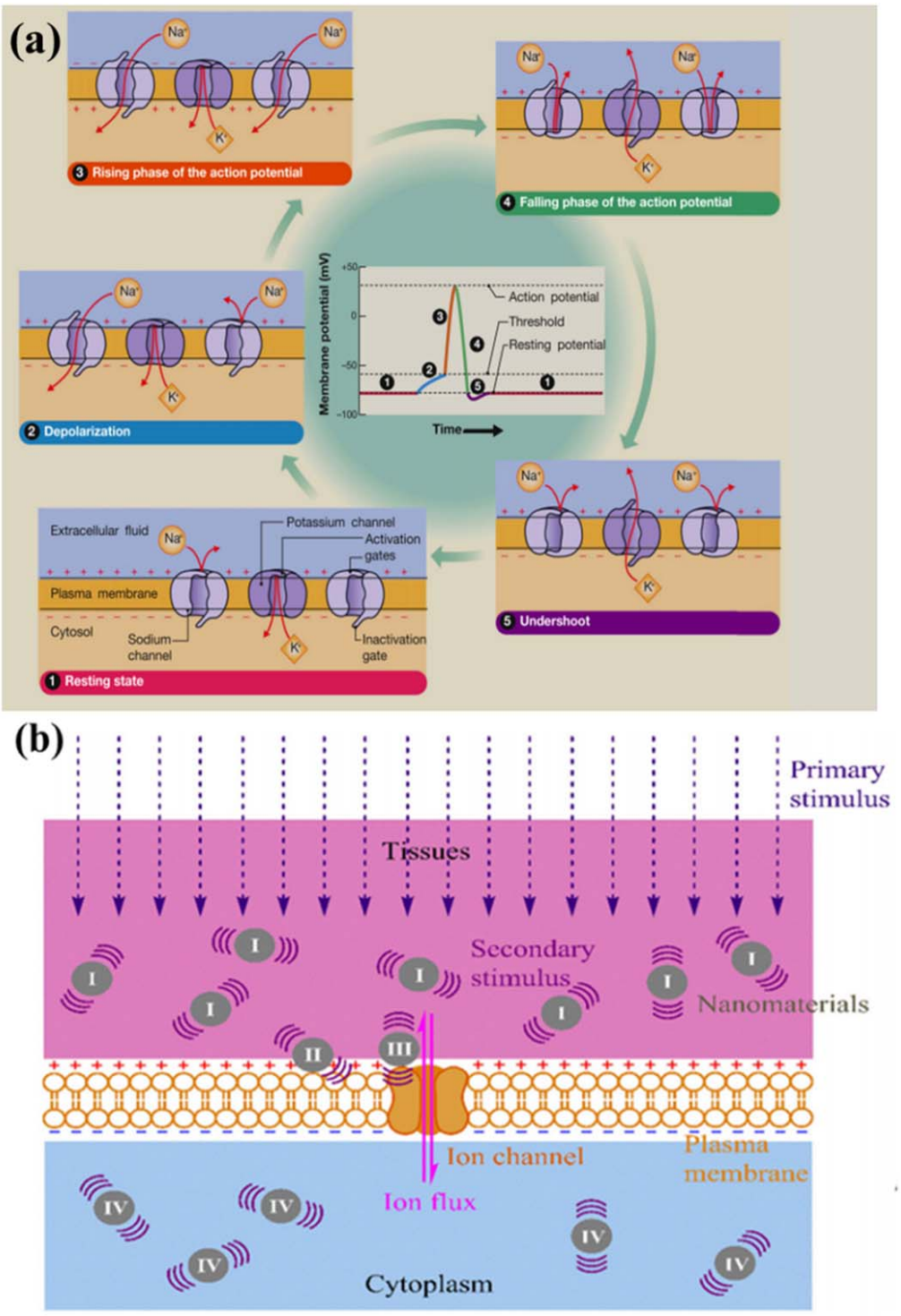

Figure 3. (a) The 5-step molecular events that generates the action potential in a neuron—resting membrane potential, depolarization, action potential peak and repolarization. Reprinted from [30], Copyright © 2011 Published by Elsevier Ltd. (b) Influx of ions due to application of an external (primary or secondary) stimulus. Reproduced from [29]. CC BY 4.0.

autofluorescence imaging [36, 37] and advanced optogenetic probes [38–40] for neural imaging. Unless it is a closed-loop stimulation and recording and/or imaging set-up [41, 42], for neural implants one must make sure that the stimulation technology is compatible with the recording set-up. For instance, as discussed earlier, DBS leads once surgically inserted cannot be monitored externally by MRI due to excessive heating of the DBS leads due to 'antenna effect'. Since neuronal signal recording is not the focus of this review, we will not introduce the mechanisms of each recording techniques. Here are some research works for readers' reference [8, 31, 32, 34, 43, 44].

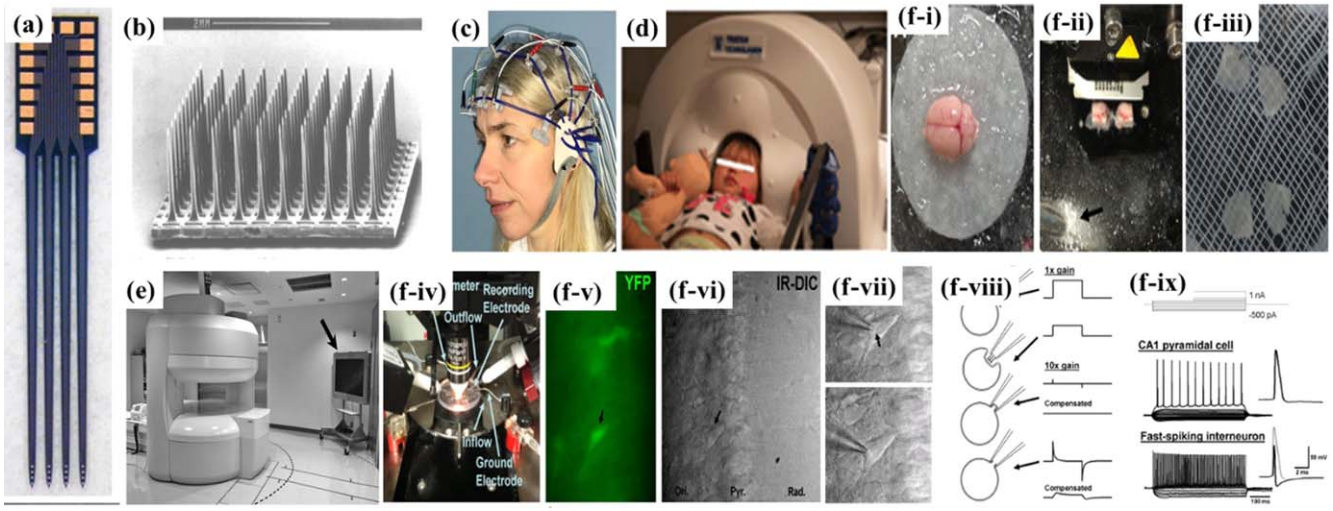

Figure 4. Invasive *in vivo* recording electrodes: (a) Michigan arrays. Reproduced from [45]. CC BY 4.0. (b) 3D Utah arrays. Reprinted from [32], Copyright © 1997 Elsevier Science Ireland Ltd. All rights reserved. Published by Elsevier Ireland Ltd. All rights reserved. Non-invasive recording and/or imaging: (c) electroencephalogram (EEG). Reproduced from [46]. CC BY 4.0. (d) Magnetoencephalogram (MEG). Reproduced from [47]. CC BY 3.0. (e) 1.2 tesla (T) open magnetoresonance imaging (MRI) equipment. Reproduced with permission from [48]. (f-i) A freshly dissected brain kept in ice. (f-ii) Hippocampal slicing of the dissected brain with a vibratome. (f-iii) After slicing, the slices are moved to warmed sucrose-ACSF. (f-iv) Patch clamp recording set-up. (f-v) Low power epifluorescent image/yellow fluorescent protein signal (YFP) in the CA1 of the hippocampus in a slice. (f-vi) Infrared differential interference contrast (IR-DIC) of the same region as that in (f-v). (f-vii) High power IR-DIC image of the soma region. (f-viii) Schematic of the major steps involving patch-clamp recording of the neuron cell. (f-ix) Patch clamp recording from different kinds of neuron cells. Reproduced with permission from [44].

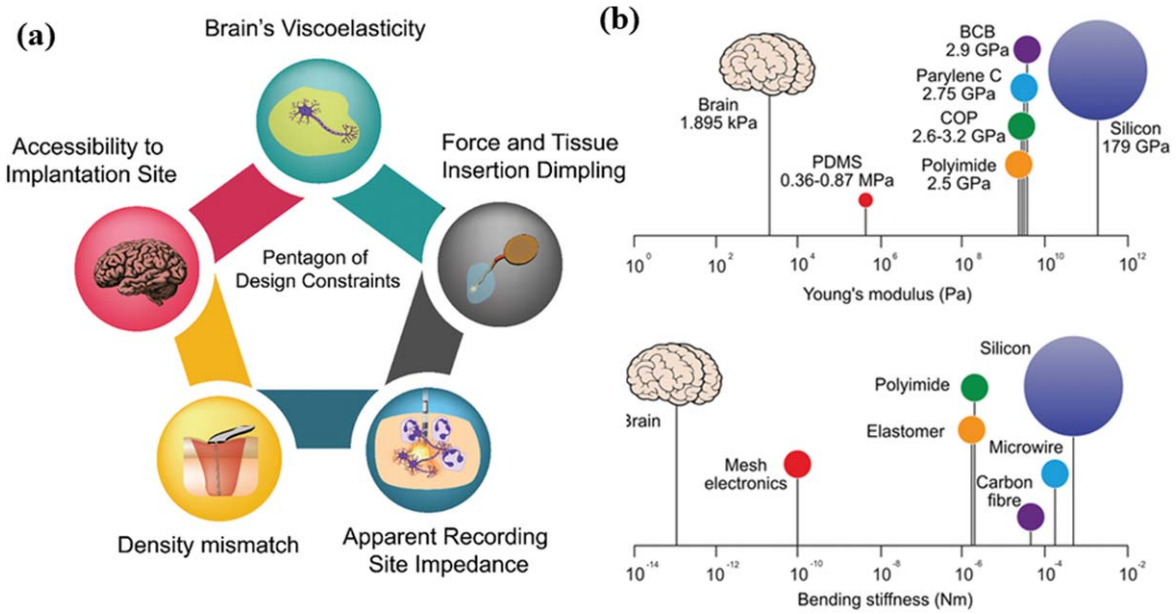

Figure 5. (a) Pentagon of design constraints by McGlynn *et al* [49]. (b) Comparison of the Young's modulus and bending stiffness of some common substrate and encapsulation materials for neural implants with respect to that of the brain tissue. Closer the value of these materials to that of the brain, better is the materialistic design for the implant. Reproduced from [49]. CC BY 4.0.

2.4. Material selection for neural prostheses

McGlynn *et al* [49] have very efficiently demonstrated the 'Pentagon of Design Constraints' in designing neuro-stimulation implants (see figure 5(a)). First vertex of the pentagon, the design and shape of these neural implants depend a lot on the accessibility of these neural implants to the implantation site. Miniaturizing these implants have been the recent focus for implant design [50–52]. However, optimization of each iteration involving the advancement of probe design and fabrication will eventually contribute to more innovation in neural probes which will be carried forward towards the future of patient care. Second vertex, selection of materials for the implant corroborating the

viscoelastic coefficient of the brain is extremely important. In terms of material selection, it is a trade-off among many factors. In terms of Young's modulus, implants made from polydimethylsiloxane (PDMS) substrates [53, 54] are preferred over benzocyclobutene (BCB) [55, 56], parylene-C [57–59], and polyimide [60–62]. Implants made from silicon substrates are the worst (see figure 5(b)). Alongside Young's modulus, one must consider the bending stiffness of the materials. Neural implants need to be of a certain stiffness for insertion but not too stiff such that it cannot be accommodated within the gyri and sulci of the brain. In terms of material selection, the same theory applies for encapsulation of these implants to improve biocompatible and be leakage-current free. Third vertex of the pentagon includes the force and tissue insertion dimpling. A successful implant in this respect is a combination of the material selected for the neural implant and the surgical technique used to insert the implant. Fourth vertex of the pentagon is extremely important to take note while designing: impedance at the site of implantation. Chronic inflammatory response from neighboring tissues have proved to be a nuance which is hard to eliminate while designing neurostimulation implants [63, 64]. After implantation, the adjacent microglial cells accumulate surrounding the implants thereby increasing the threshold required for activation of these neuronal cells. This is also the same reason why most DBS implants need to be replaced every 2 years through a surgical procedure [13, 65]. The fifth and the final vertex of McGlynn *et al*'s pentagon for neural implant design constraint is density mismatch between the brain tissue and the designed neural implant. This vertex is in direct correlation with the second vertex. Overall, this pentagon has covered the basic points for implant design in the brain-computer interface.

3. Review on micromagnetic neurostimulation

The feasibility of magnetic stimulation on biological tissues, more precisely human visual cortex, was first demonstrated by Jacques d'Arsonval in 1896 [66], followed by Silvanus P. Thompson in 1910 [67]. In this regard, the concept of employing magnetic μcoils as potential neurostimulators is relatively new. They are DBS-like-'implants' [1] but operate on the 'physics'-of-TMS [68], i.e. on applying an electric current through the μcoils (an inductive load) to generate a 'highly permeable' [69] time-varying magnetic field that ultimately induces an electric field. This induced electric field is spatially asymmetric and has been reported to have the potential of selectively stimulating neurons [16]. The most fascinating property of this induced electric field in neurostimulation is that it is not in direct galvanic contact with the neuron tissues. Thus, the magnetic neurostimulation devices are expected to remain protected from biofouling nuances [70, 71]. We will investigate the pros and cons of micromagnetic neurostimulation in section 6 where we have discussed the advantages and disadvantages in details.

Bonmassar *et al* [15] had pioneered micro-magnetic stimulation (μMS) by using commercially available RF inductors to stimulate neurons (see figure 1(c)). Following their work, the same group of researchers and several other research groups worldwide fabricated customized μcoils [16, 72], including planar [17], trapezoidal [16], figure-of-eight planar [73] or solenoidal [15, 74], even solenoids with magnetic cores [75] or V-shaped bent wires [16]. They provide selective spatial control of different kinds of neurons, for both *in vitro* and *in vivo* applications: L5 pyramidal neurons [76], intracortical neurons [16], inferior colliculus (IC) [74] neurons and hippocampal CA3-CA1 synaptic pathway [77]. Also, these μcoils are expected to be MRI compatible when turned off, as there is no galvanic contact with adjacent tissues, thereby limiting the amount of heat generation [7]. However, the power of operation of these μcoils is three orders higher than DBS leads [15] and, being sub-mm sized, achieving cellular-level neurostimulation is impossible.

3.1. Theory of micromagnetic neurostimulation

The principle of μMS is based on Faraday's law of electromagnetic induction [6, 15, 74, 78]:

$$\nabla \times E = -\frac{\partial B}{\partial t}, \tag{2}$$

where, $\boldsymbol{E}$ is the induced electric field and $\boldsymbol{B}$ is the magnetic flux density. Using the definition of the above equation,

$$B = \nabla \times \boldsymbol{A} \tag{3}$$

and

$$E = -\frac{\partial \boldsymbol{A}}{\partial t} - \nabla V, \tag{4}$$

where $\boldsymbol{E}$ is dependent on both the vector electric potential, $\boldsymbol{A}$, and magnetic scalar potential, V, in a time-varying manner. Biological tissues are excited due to application of a magnetic field, $\boldsymbol{H}$, following Ampere's law [78]:

$$\nabla \times H = J, \tag{5}$$

where, $\boldsymbol{J}$ is the current density flowing through the biological tissues after its activation. Here, $\boldsymbol{H}$ and $\boldsymbol{B}$ are related by:

$$B = \mu H, \tag{6}$$

where μ is the permeability of the biological tissue medium (same as that of air). The total current density $\boldsymbol{J}$ is expressed as the sum of the conduction current $\sigma \boldsymbol{E}$ and the externally applied current, J_e:

$$J = \sigma E + J_e. \tag{7}$$

This flow of current within the neurons implies activation of the neurons. Therefore, it must be noted that for μMS, there is no threshold magnetic field for neurostimulation. A combination of magnetic field, the tissue permeability, the device dimension, and the area of the region available for neurostimulation generates the induced electric field to stimulate the neurons. The goal is to have this induced electric field, its strength and duration lie on the strength–duration curve in figure 2(a).

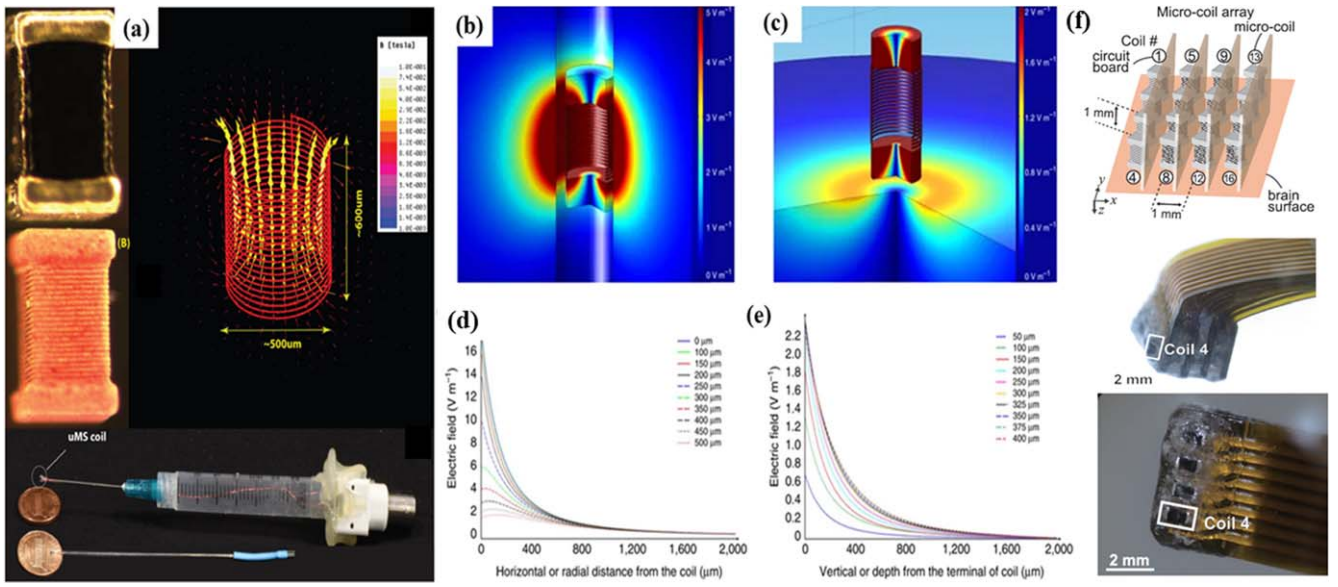

Figure 6. Commercially available μcoil set-up in micromagnetic neurostimulation. (a) The prototype for the commercially available magnetic μcoil mounted at the tip of the syringe (micromanipulator) with magnetic field distribution. Electromagnetic simulations on COMSOL AC/DC Module demonstrating 3D electric field distribution along the horizontal direction (b); along the vertical direction of the μcoil (c). Spatial attenuation starting 100 μm along the horizontal or radial distance (d) and 100 μm along the vertical or depth (e) of the terminal of the μcoil. Reproduced from [6]. CC BY 4.0. & Reprinted by permission from Springer Nature Customer Service Centre GmbH: Springer Nature, Nature Communications, [15], Copyright © 2012, The Author(s) (f) Schematic representation of the arrangement of 16 commercially available inductors in the configuration of 4 × 4 array on a plane of $z = 0$ mm, thereby forming a multi-solenoid system. The front (middle image) and side views (bottom image) of the same system are represented in the following images. Reproduced from [81]. © IOP Publishing Ltd. All rights reserved.

3.2. Microcoil device implants, the driving circuitry and neural responses

3.2.1. Commercial microcoils. For the first time, in the year of 2012, Bonmassar *et al* [15] had shown the pragmatic feasibility of μMS using magnetic μcoils. Their work and some other follow-up simulations and/or experimental works from several other groups [6, 74, 79, 80] used commercially available, air-cored MEMS RF 0402 inductor (Model No. ELJ-RFR10JFB, Panasonic Electronic Devices Corporation), with 21 turns, 100 nH inductance, 5.5 Ω maximum DC resistance, and 400 × 400 × 600 μm dimension as the magnetic μcoils (see figure 6(a)). Electromagnetic simulations on COMSOL AC/DC Module (see figures 6(b)–(d)) have shown that the commercial μcoils generate higher electric field along the horizontal or radial distance of the μcoil compared to its vertical or depth. Upon application of a 10 A current, the spatial distributions for magnetic flux density (in mT) and induced voltage (in mV) spatial distributions in the y–z plane are shown in figures 6(b) and (c). However, the induced electric field attenuates rapidly from the surface of the μcoil along both horizontal and vertical directions (see figures 6(d) and (e)). This in turn has led to orientation dependent activation of neurons by these μcoils contributing to a unique advantage of micromagnetic stimulation: selectivity (see figures 7(a)–(c)). This orientation dependence of the μcoils has been reported in many works [15, 74, 79]. Even a controversy on the most suitable orientation of the commercially available μcoils has been reported recently. For instance, it has been reported by Osanai *et al* [79] that Type A orientation (see figure 7(b)) can stimulate neurons *in vivo*, Type B orientation cannot (see figure 7(b)). The justification for this preference in orientation being, the x-component of the induced electric field become negligible in Type B orientation thereby hindering any neuron response. This result was in direct controversy with respect to the most suitable orientation for neurostimulation reported by several research groups prior to that [15, 74, 76]. Their reports, although in an *in vitro* setting, suggest that the Type B orientation is the most preferable choice for neurostimulation, Type A being the second choice (see figure 7(c)). This opens a huge research field in terms of experiments as well as numerical modeling to investigate which orientation of the μcoils is the most preferred. There are several factors which might cause change in preference of the orientation of the μcoils for neurostimulation. For instance, for both *in vitro* and *in vivo* experiments, the kind of neurons being stimulated (excitatory or inhibitory) or even the experimental setting in which the neuron responses are being recorded might affect the decision regarding which is the most preferable orientation of commercial μcoils for micromagnetic neurostimulation. In this respect, the most recent work on micromagnetic stimulation where Saha *et al* [77] is extremely relevant. They studied the effect of these commercial μcoils on eliciting excitatory post synaptic responses (EPSPs) from the hippocampal CA3-CA1 synaptic pathway. A major observation of their work was that in *in vitro* settings too, Type A orientation has been more

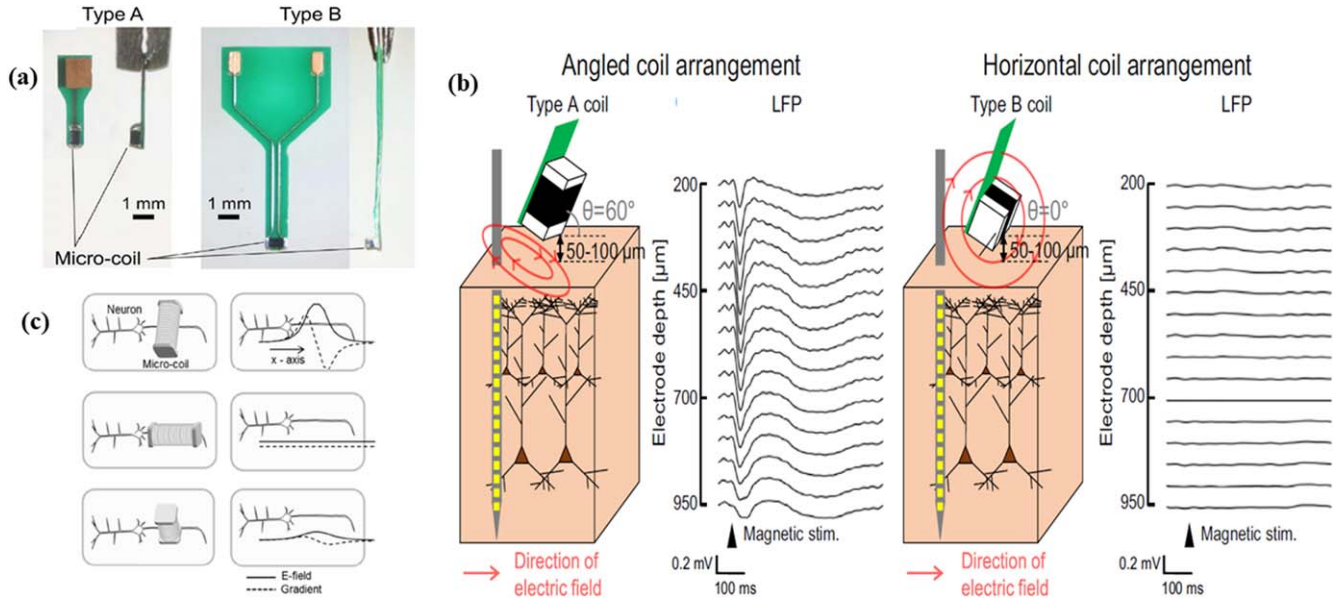

Figure 7. Demonstration of orientation dependent activation of neurons by commercially available solenoidal μcoils by Minusa *et al*. (a) Mounting commercially available μcoils on a PCB in two orientations, Type A and Type B. (b) Osanai *et al* reported that Type A orientation shows local field potential (LFP) recording, meaning successful activation of neurons; whereas, Type B orientation shows no LFP, meaning no activation of neurons, *in vivo*. Reprinted from [79], © 2017 IBRO. Published by Elsevier Ltd. All rights reserved. (c) On the contrary, Lee *et al* reported that for *in vitro* activation of pyramidal neurons, Type B orientation was most suitable; Type A orientation was the second choice. © 2014 IEEE. Reprinted, with permission, from [82].

successful in eliciting EPSPs. They justified their findings through both modeling as well as experimental efforts.

Furthermore, in the year of 2019, Minusa *et al* [81] arranged 16 of these commercially available inductors in a 4×4 array on a flex printed circuit board (PCB) and studied the influence on the auditory cortex of rodent brain (see figure 6(f)). Along the line of investigation for commercially available μcoils for implantable micromagnetic neurostimulation, several groups across the world have contributed in the past decade, each having their unique experimental approaches of μcoil mounting and neuron recording set-up [6, 74, 79, 83–85]. However, in this field of research one thing has been constant: numerical studies for generating the spatial heatmaps of the magnetic flux density and the induced electric fields from the respective μcoils. One possible reason may be that because these implants are sub-mm in size, it is difficult to customize a set-up to measure the magnetic field, let alone measure the induced electric field from these μcoils. Hence, numerical simulation on ANSYS-Maxwell or COMSOL AC/DC module is beneficial in this respect. Nevertheless, Minusa *et al* [83] has been successful in custom-building such a set-up where the induced electric field generated from these μcoils are measured by the electromotive force (emf) generated within the custom-built search coil. Even, Khalifa *et al* [75] very recently used the nitrogen vacancy in diamond as a magnetometer to measure the magnetic field coming out of these μcoils. This further corroborates the fact that it is indeed difficult to measure the microscale magnetic field generated from these μcoils.

In an electrical circuit, μcoils behave as inductive loads. Since in an inductor, the voltage and the current are not necessarily in the same phase, simply passing a current through an inductive load is not enough to drive the μcoils. To drive an inductive load, we need a voltage source, which for the μcoils in μMS reported by researchers from Harvard Medical School is the function generator (AFG3021B, Tektronix Inc.). Researchers from Hokkaido University used a digital acquisition (DAQ) as the signal source [79, 81, 83]. However, the function generator is equipped to drive a resistive load of approximately 50 Ω which causes the necessity of a special kind of amplifier/driver along with the voltage source. Hence, the μMS drive consists of a function generator connected to a 1000 W MOSFET power amplifier of gain which varies across different literature [15, 16, 83] (see figure 8(a)). As per the published reports for μMS, this gain ranges between 2.3 V/V and 5.6 V/V gain of bandwidth 70 kHz (PB717X, Pyramid Inc.). The various current waveforms that are applied through the μcoils through this driving circuitry has been summarized in table 1 (see figure 8(b)). The reason for selection of this specific class-D power amplifier for μMS studies is unknown. However, it seems like μMS requires a high current to elicit neuron responses and this amplifier provides an extremely high current rating. On the other hand, very recently, Dong *et al* [84] has preferred to custom-design the μcoil driving circuitry using audio amplifier integrated circuits (ICs) and has shown how μMS can stop epileptic discharges from hippocampal brain slices.

Figure 8(c) demonstrates the *in vivo* neural response from the inferior colliculus (IC) neurons of the dorsal cochlear nucleus (DCN) of adult male Syrian golden hamsters aged 12–17 weeks, before (figure 8(c), top) and after euthanasia (figure 8(c), bottom). Multi-unit measurements were performed through rigorous process of filtering and amplification

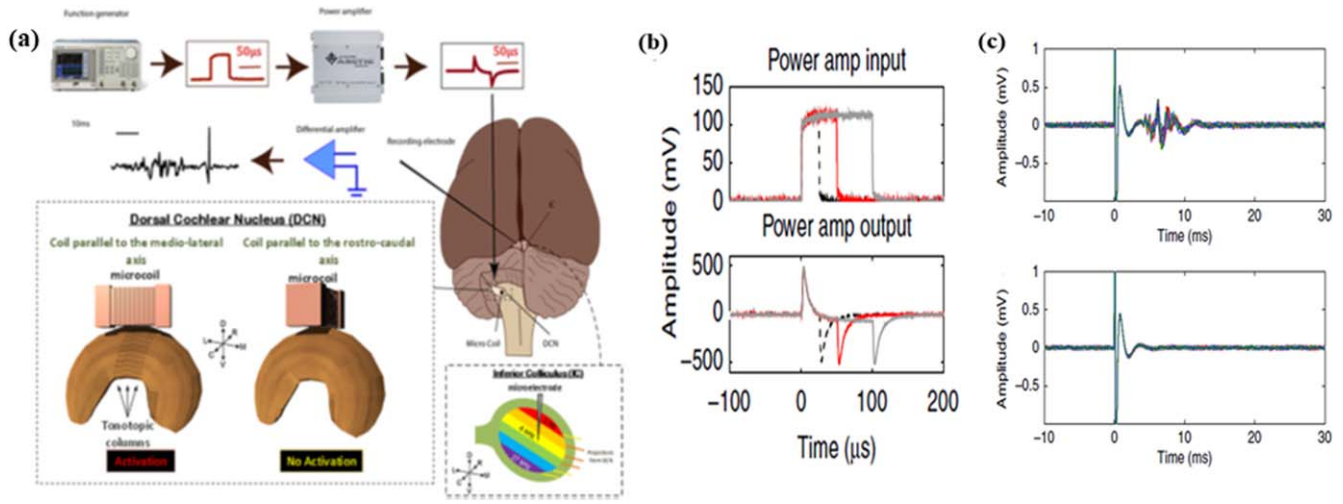

Figure 8. (a) μMS drive for μcoils consisting of a function generator and a power amplifier. (b) The power amplifier input and output of the μMS drive. The power amplifier output is given as an input to the μcoil. (c) *in vivo* neural response because of μMS before (top) and after (bottom) euthanasia of the animals. The results are averaged over 10 repeats of measurements. Reproduced from [6]. CC BY 4.0. Reprinted by permission from Springer Nature Customer Service Centre GmbH: Springer Nature, Nature Communications, [74], Copyright © 2013, Nature Publishing Group, a division of Macmillan Publishers Limited. All Rights Reserved.

of the signal using recording electrodes with an impedance of 0.4–0.5 MΩ. In general, as shown in figure 8(c) (top), it is observed that the neurons show a latent response. A stimulation artefact is observed immediately on application of the stimulus, followed by firing of neurons after 8 ms of stimulus application which continues up to 15 ms. Raster plots in figure 9(a) show that for a constant stimulus duration of 50 μs, out of three different amplitudes of 100 mV, 300 mV and 600 mV, as the stimulus amplitude increases, the probability of neuron firing increases significantly. On the contrary, the raster plots in figure 9(b) where a constant stimulus amplitude of 300 mV and varying stimulus durations of 25 μs, 50 μs and 100 μs were applied, it shows a maximum neuronal firing probability at 50 μs and comparatively reduced firing probability in the other two cases. This *in vivo* study implies that both the stimulus strength and duration through the μcoils jointly influence the neuronal response.

In general, some conclusions can be made with respect to implantable μMS. The *in vitro* studies [6, 15] showed that μMS is highly dependent on the orientation of the μcoil, varied with the amplitude and time duration of the μMS drive. The *in vivo* studies [16, 78] confirmed all the observations in the *in vitro* studies, in addition to showing that μMS can elicit neuronal stimulation in an interconnected neural circuit (see figure 8(a), where μMS was made at DCN but responses were recorded at IC neurons) and is not restricted to local circuitry (for instance the *in vitro* tissue slices).

3.2.2. Custom-fabricated microcoils: V-shaped. The commercial μcoils discussed in section 3.2.1 require an extremely high input current for suitable performance as neurostimulators. For μcoils being implantable devices, such high current of operation is unacceptable as this would cause detrimental thermal effects on neuronal tissues. This motivated the research groups to fabricate customized copper (Cu) [16] or gold (Au) [17] μcoils. Park *et al* [74] reported *in vivo* experimental results on sputtered Cu coils of dimensions 10 μm wide × 2 μm thick on a Si/SiO_2 substrate of cross-sectional area 50 μm × 50 μm. The Cu coils were passivated by a 300 nm thick SiO_2 to prevent leakage as well as an attempt at making the Cu μcoils biocompatible (see figure 10(a)). However, it is likely that coils made of Cu will continue to remain cytotoxic [88, 89]. Table 1 covers the detail of the *in vivo* application of this μcoil.

3.2.3. Custom-fabricated microcoils: planar microcoil. In that perspective, the 6 × 6 planar, electroplated Au μcoil arrays fabricated by Rizou *et al* [17] in figure 10(b) seems to be a better alternative. Each planar Au μcoil has 5 turns and is made of 1.7 μm thick, 2 μm wide wires and with 2 μm pitch. The fabricated μcoils have the following specifications: $R_{dc} = 22\ \Omega, L = 1.69\ \mu$H, and $C = 14$ nF, considering the self-resonant frequency to be at 10 MHz. For a current of 9 mA, the simulated spatial distribution of the magnetic flux density (in mT) and the induced electric field density (in mV) at 800 nm above the μcoil surface is shown in figure 10(c). Simulations show that these planar μcoils, being smaller in dimension compared to the commercial μcoils, generate more localized and larger electric field for neurostimulation. Table 1 covers the detail of the *in vivo* application of this μcoil. Yet another new design of planar μcoils for micromagnetic neurostimulation have been developed by Saha *et al* [90, 91], the very first of its kind in terms of design, materials and study of its application. Those new neurostimulation planar μcoils are currently being investigated for cellular-level stimulation by culturing neuron cells directly on these devices.

3.2.4. Custom-fabricated planar microcoils with soft magnetic material. The μcoils proposed by Ramadan *et al* [92], Niarchos *et al* [93] (see figures 11(a) and (b)) and Dong *et al*

Table 1. Summary of reports published in the field of micromagnetic neurostimulation (μMS)

Coils	Length × width × thickness (in mm)	Driving circuitry and neurological disease treatment (if any)	No. of coils	Experimental setting	Stimulation site	Distance between coil and neuron tissue	Neuron response recording set-up	Reference
Commercial microcoil (Panasonic, ELJ-RFR10JFB)	1 × 0.5 × 0.5	Positive and negative pulses of frequency 1 Hz; Amplitudes ranging from 0–10 V in steps of 0.5 V	One	*in vitro*	Rabbit retinal ganglion cells	300 ± 50 μm	Patch-clamp	[15]
Commercial microcoil (Panasonic, ELJ-RFR10JFB)	1 × 0.5 × 0.5	Monophasic rectangular stimulation pulses with different pulse-widths (25–100 μsec) and amplitude (100 mV – 600 mV)	One	*in vivo*	Dorsal cochlear nucleus (DCN)	∼100 μm dorsal	Microelectrode + oscilloscope	[74]
Commercial microcoil (Panasonic, ELJ-RFR10JFB)	1 × 0.5 × 0.5	Sinusoidal bursts of amplitude (0–5.005 V) of frequency 500 Hz for an interval of 30 s; Each burst separated by 20 s	One	*in vitro*	Prefrontal cortex (PFC) L5 Pyramidal neurons	200 μm away from the center of soma	Patch-Clamp	[86]
V-shaped Cu microcoil	2 × 0.1 × 0.05	Single full period 3-kHz sinusoid waveform of amplitude 0–200 mv; Single sinusoids of 5 or 10 pulses delivered at 10 and 100 Hz resp.; repetitive stimulation at 1 pulse/sec delivered for 10 s	One	*in vitro* and *in vivo*	M1 L5 pyramidal neurons	50–160 μm from the soma	Calcium fluorescence imaging and analysis (*in vitro*); detection of whisker movements in mice (*in vivo*)	[16]
Commercial microcoil (Panasonic, ELJ-RFR10JFB)	1 × 0.5 × 0.5	Monophasic rectangular pulses with varied pulse widths and amplitudes	One	Finite element method (FEM) + NEURON-based modeling + *in vivo* experiments	Syrian golden hampsters	∼20 μm	Microelectrode + oscilloscope	[6]
Commercial microcoil (Panasonic, ELJ-RFR10JFB)	1 × 0.5 × 0.5	Rectangular pulses of pulse width 0.5 ms, amplitude 5 V, stimulation frequency 10 times/trial and stimulation interval 6 s	One	*in vivo*	Auditory cortex	—	Flavoprotein autofluorescence imaging	[79, 83]
Commercial microcoil (Panasonic, ELJ-RFR10JFB)	1 × 0.5 × 0.5	Rectangular pulses of pulse width 0.5 ms, amplitude 5 V, stimulation frequency 10 times/trial and stimulation interval 6 s	4 × 4 array	*in vivo*	Primary auditory cortex	—	Microelectrode + oscilloscope	[81]
Commercial microcoil (TDK, MLG1005SR10JTD2)	1 × 0.5 × 0.5	Pulses of width 1 ms and duration 10–30 s were generated at a frequency between 20 Hz – 400 Hz.	One	*in vitro*	Hippocampal CA3 region	500 μm	Patch-clamp	[85]
Commercial microcoil (Murata, LQP02TN39NJ02)	0.4 × 0.2 × 0.2	Portable microcoil driving circuit with an amplitude of 10 V and 70 kHz frequency; Treatment of epilepsy simulations	One	*in vitro*	Hippocampal CA3 region	200 μm	Multichannel bioelectric recording set-up	[84]
F/C structured planar microcoil	0.1 × 0.1 × 0.002	—	One	—	—	—	—	[87]
Planar microcoil array	0.05 × 0.05 × 0.0017	FEM + NEURON simulations	6 × 6 array	—	—	—	—	[17]

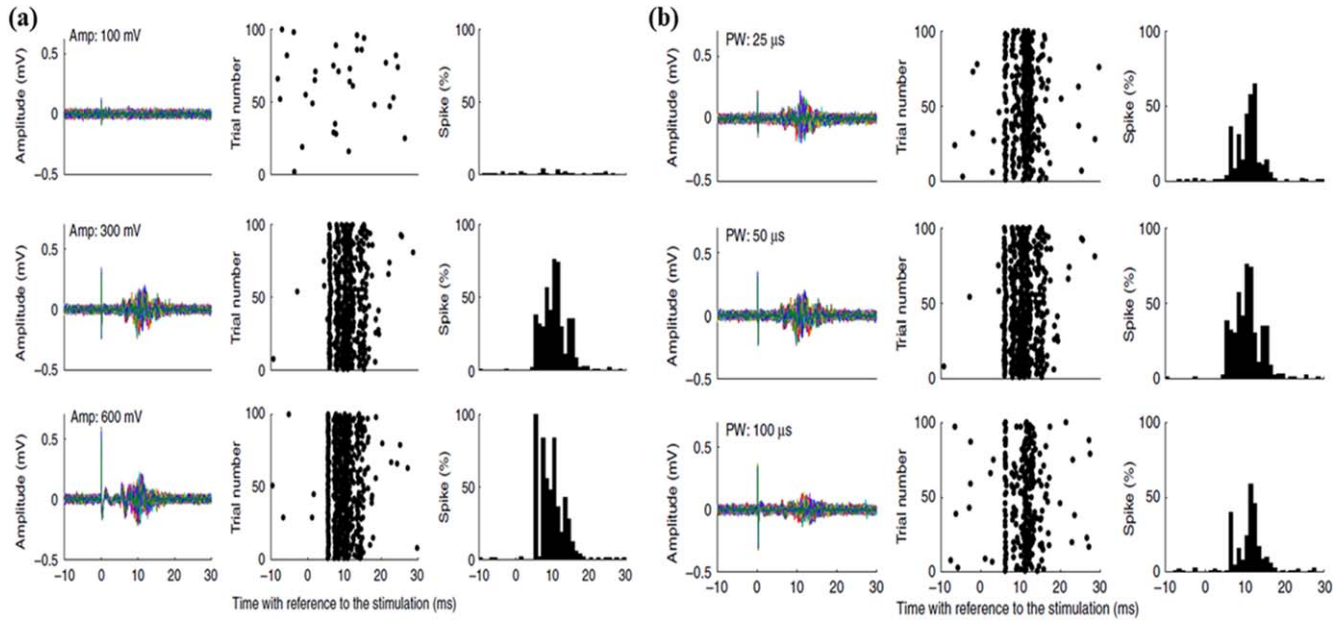

Figure 9. (a) *In vivo* neural response with varying stimulation amplitude but constant stimulation pulse width at 50 μs and, (b) varying stimulus pulse width with a constant amplitude at 300 mV. Reprinted by permission from Springer Nature Customer Service Centre GmbH: Springer Nature, Nature Communications, [74], Copyright © 2013, Nature Publishing Group, a division of Macmillan Publishers Limited. All Rights Reserved.

[94] (see figures 11 (c) and (d)) have a soft magnetic core or an array of soft magnetic pillars surrounded by planar μcoil. The purpose of the soft magnetic core is to provide a larger, more spatially concentrated magnetic flux from the μcoils. Although these μcoils are commonly used as magnetic actuators, they can act as potential neurostimulators. Furthermore, a 6×6 array of gold μcoils (shown in figures 10(b) and (c)) were fabricated by Rizou *et al* [17] specifically for implantable micromagnetic stimulation (μMS). Inspired by the combined efforts of Ramadan *et al* [92] and Rizou *et al* [17], there lies the possibility of an implantable nanopatterned soft magnetic material-based μcoil that has an array of electroplated soft magnetic permalloy ($Ni_{80}Fe_{20}$) cylinders of a specific diameter and height. The planar Au coils spiraling around the nanopatterned soft magnetic pillars consist of some desired number of turns, wire diameter and thickness. The idea for this kind of nanopatterned soft magnetic material-based μcoil is to optimize the aspect ratio of the cylindrical permalloy pillar such that the magnetic field generated by the planar coil alone is equal to or less than the coercive field of the permalloy pillar. This calls for extensive micromagnetic calculations (possible on platforms such as OOMMF [95] or Mumax3 [96]) with varying aspect ratios such that the coercive field of the permalloy pillar is as low as possible and it specifically has a linear MH curve, i.e. no hysteresis loop at the center. The other part of the plan will be to optimize the number of turns of the μcoil and the current of operation for the μcoil through electromagnetic simulation studies on COMSOL AC/DC Module (https://www.comsol.com/acdc-module) or ANSYS Maxwell software (https://www.ansys.com/products/electronics/ansys-maxwell). This will help in determining the final dimensions of the nanopatterned μcoil associated with neurostimulation in addition to the number of nanopatterns that will be required to generate the required magnetic field, which in turn generates the induced electric field for neurostimulation. The ultra-low power of operation coupled with high spatial resolution of tissue stimulation makes the μcoils reported by Ramadan *et al* [92] promising candidates for neurostimulation. The recent soft magnetic material cored solenoidal coils reported by Khalifa *et al* [75] further strengthens the concept. A very similar approach to simulate such nanopatterned soft magnetic material-based μcoils generating intensified and focused magnetic flux density at these pillars (see figure 11(d)) have been reported by Tian *et al* [87] and Dong *et al* [94]. However, strong experimental evidence to support this type of μcoils in micromagnetic neurostimulation is missing in literature thereby providing ample scope for innovation. Recently, a patent has been filed by Wang *et al* [97] claiming the invention of nanopatterned soft magnetic material-based μcoil (nSMMcoil) for ultra-low power, cellular-level neurostimulation.

3.2.5. Printing microcoils on flexible substrates. All the literatures reported so far used either commercially available or microfabricated μcoils to demonstrate micromagnetic neurostimulation. In view of fabrication methods of μcoils, Le *et al* [98] have recently done an excellent job in summarizing the MEMS inductor fabrication techniques focusing on applications in power electronics and neurotechnologies. The traditional method to fabricate μcoils is time consuming and expensive. However, there exists some extremely cost-effective, fast and reproduceable methods of fabricating μcoils using additive manufacturing methods, including inkjet printing, aerosol jet printing, and 3D printing. For instance, Sarreal *et al* [99] used aerosol jet

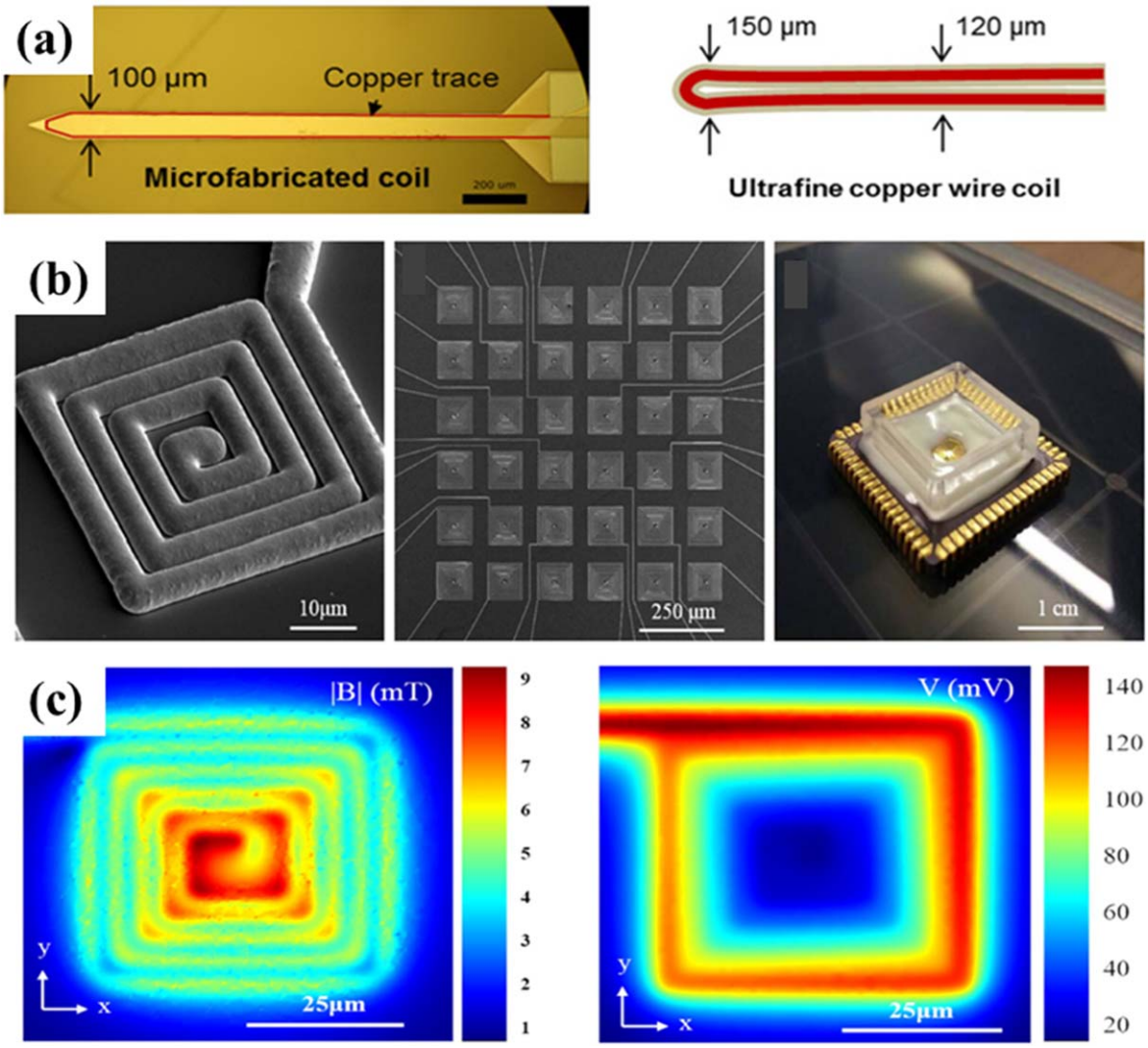

Figure 10. (a) Custom fabricated Cu μcoils. From [16]. Reprinted with permission from AAAS. (b) 6 $\times$ 6 planar gold μcoils, each of 5 turns and 1.5 μm thick, 2 μm width and 2 μm spacing for μMS. (c) Magnetic flux density (in mT) and induced voltage spatial distribution (in mV) for one planar gold μcoil at a distance of 800 nm above the μcoil surface. Reproduced from [17].

printing techniques to demonstrate micromagnetic cochlear stimulation using silver-nanoparticle μcoil, as shown in figure 12. Zhang *et al* [100] fabricated a copper based flexible micro inductive coil on paper. Other probable techniques for custom fabrication of μcoils using additive manufacturing techniques are available from Ha *et al* [101], Meier *et al* [102] and Wang *et al* [103].

3.3. Treatment of neurological disorders using micromagnetic neurostimulation

Most of the work on micromagnetic neurostimulation has been focused on designing custom-made μcoils and recording electrophysiological responses, both *in vivo* and *in vitro* on specific neuron models. However, attempts have been made to investigate the use of commercial μcoils for the treatment of epilepsy. Lee *et al* [104] showed that single pulses through commercial μcoils generated weak and inconsistent subthalamic nucleus activity but repetitive stimulation effectively suppressed the activities in $\sim$70% of the targeted neurons. The suppression of the subthalamic activity reported was latent in general which was inversely correlated to the stimulus energy of the waveform. They reported larger amplitudes and lower frequencies triggered the fastest onset of suppression. Dong *et al* [84] reported suppression of epileptiform discharges in rat hippocampal slices through high frequency stimulation from the commercial μcoils. Skach *et al* [105] reported reversible axonal blockage of unmyelinated axons of the buccal ganglia (see figures 13(a) and (b)) from the marine mollusk *Aplysia California* using commercial μcoils operating at a high frequency supported by simulations (see figures 13(c)–(e)). Ye *et al* [106] reported somatic inhibition using the same neuron model and similar commercial μcoil set-up. Both works further highlight the potential of micromagnetic neurostimulation as a promising treatment for epilepsy. This technology is infant in its nature and has immense scope for finding its application in other fields of brain disorder treatments.

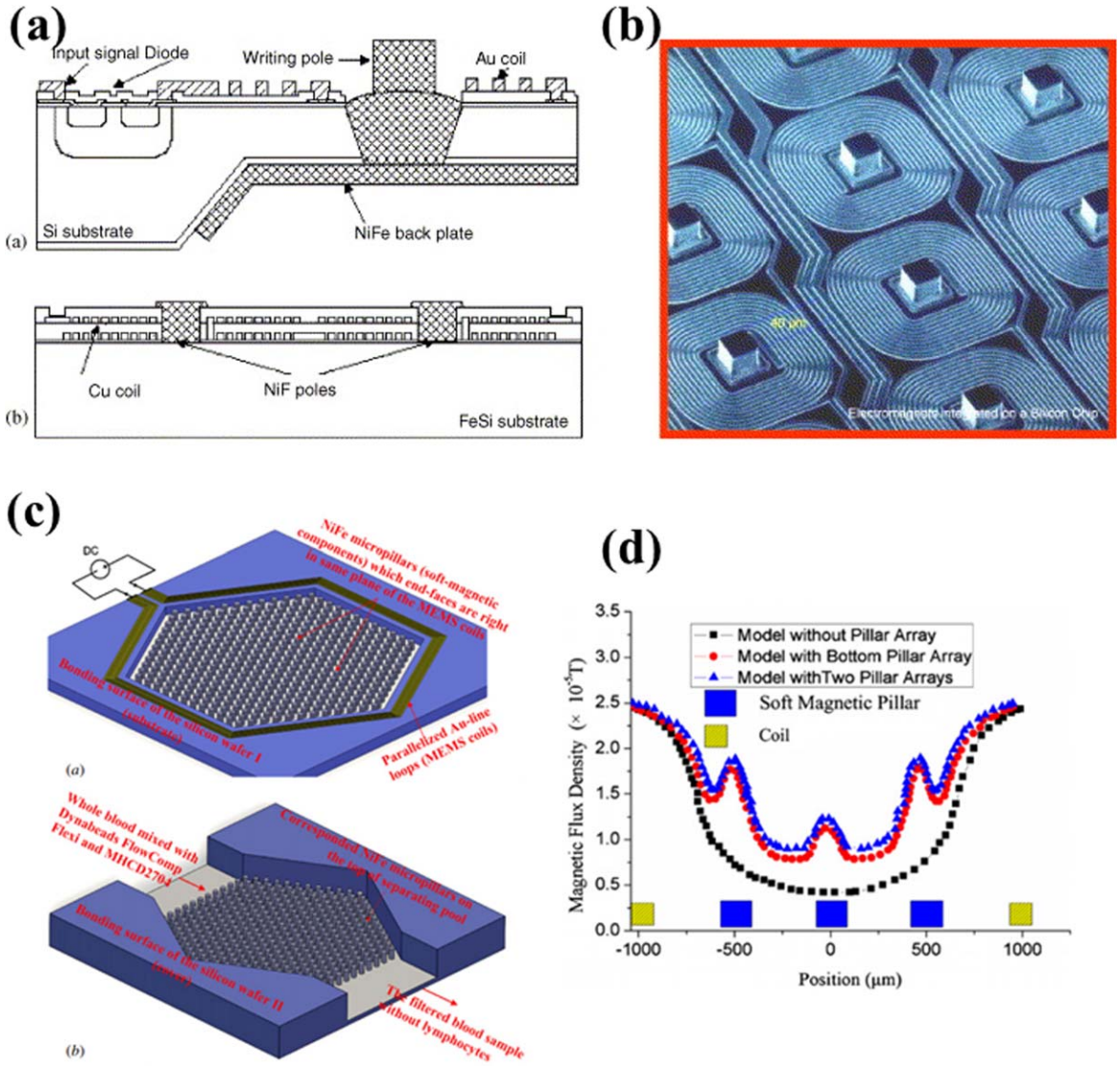

Figure 11. (a) Cross-section of single-layer gold coils with electroplated soft magnetic material core. (b) Multilayer copper coils with FeSi (another soft magnetic material) bulk and electroplated core. They can be potential candidates for neurostimulation. Reprinted from [93], Copyright © 2003 Published by Elsevier B.V. (c) Designed to be a magnetic separator with MEMs coils surrounding soft magnetic pillar array. This design can totally be applied for cellular-level magnetic neurostimulator design. (d) The increased magnetic flux density (in T) with and without soft magnetic pillar arrays. Reproduced from [94]. © IOP Publishing Ltd. All rights reserved.

4. Spintronic nanodevices in micromagnetic neurostimulation

The spintronic nanodevice is one type of nanomaterial that utilizes the intrinsic spin of the electron and its associated magnetic moment. The topic of spintronics emerged in the 1980s starting with the discovery of spin magnetization in metals [107] and the giant magnetoresistance (GMR) effect in multilayered thin films [108]. In addition to the fundamental electronic charges of electrons, the electron spins have been exploited as an additional degree of freedom and actively applied in different areas such as data storage, quantum computing, neuromorphic computing [109–115] etc. The interplay of electron spins with their motion inside a potential (in the form of electric and/or magnetic) can be fine-tuned to generate a time-varying magnetic fields. Which, as a result, generates a localized, time-varying electric field. In this section, we will review the recent advances in using spintronic nanodevices for neurostimulation.

In 2016, Wang *et al* [116] had given a proof-of-concept for a spintronic neurostimulator using current driven domain wall motion through a photolithography patterned magnetic nanowire. The working principle for spintronic neurostimulators is where the electric field for neurostimulation is induced by the movement of magnetic domain walls inside the stational magnetic nanowires. Spintronic nanodevices operate in the ultra-low power regime [117, 118] and can be fabricated onto flexible biocompatible substrates [119, 120]. Therefore, in addition to showing all the functionalities of μMS, spintronic neurostimulators promise to reduce thermal effects on neurons. The nanometer-size of these spintronic nanodevices allow cellular-level neurostimulation.

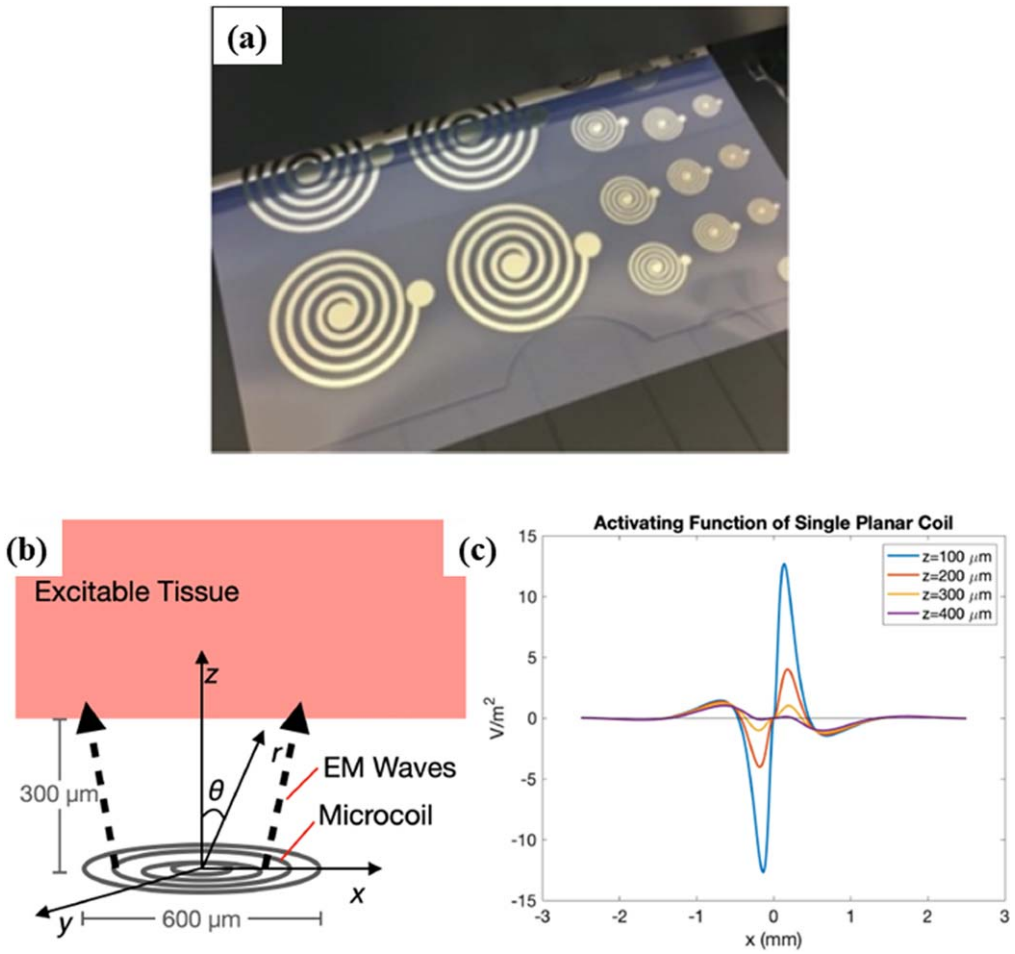

Figure 12. (a) Printed μcoils on flexible substrates where the largest coil has a diameter of 60 mm as reported by Sarreal *et al* for its application as a cochlear stimulating implant. (b) The co-ordinate system for activating excitable tissues for the microcoil. (c) The plot representing the spatial positions where the tissues are likely to be excited by the μcoil carrying a current of 1 A. For instance, the neurons located at the center of the coil will not be stimulated. Reproduced from [99]. CC BY 4.0.

Furthermore, flexible biocompatible substrates facilitate better fit in the grooves of the brain (i.e. gyri and sulci).

4.1. Magnetic nanowire neurostimulator (MNNS)

In 2016, the feasibility of magnetic neurostimulation due to displacement of domain walls through magnetic nanowires had been proposed by Wang *et al* [116]. Domain walls are the interface between neighboring magnetic domains. Domains are nanostructures in thin films where the magnetization in each domain is uniform while the magnetizations of different domains may point in different directions. The magnetization directions change from one domain to another through domain walls. On application of an external magnetic field or a charge current or a combination of both, these domain walls displace as a result of Zeeman energy and spin transfer torque (STT) [121]. STT is an effect in which the magnetization of the magnetic layer is modified using a spin-polarized current. Figures 14(a)–(i) shows the schematic of a magnetic nanowire-based neurostimulator (MNNS) as reported by Su *et al* [18]. Figures 14(a)–(ii) shows the magnetic stray fields generated by the perpendicular transverse and transverse domain walls in a magnetic nanowire, respectively. By applying a current pulse of density 10^{12}–1013 A m^{-2} along the long axis of the permalloy nanowires, the domain wall moves along the magnetic nanowire. The velocity of the domain walls is dependent on the amplitude and the direction of the applied current density [122, 123]. The stray fields from domain walls at the nanowire surface are on the order of 10^5 A m^{-1}. The stray fields generated as a result of this displacement have been widely used to switch the local magnetization [124–126]. Following Faraday's law, this displacement of domain walls (as well as the stray fields) induce a localized electric field. However, this stray field attenuates fast from the surface of nanowire with distance.

Su *et al* has used Object Oriented Micromagnetic Framework (OOMMF) [95] to calculate the intensity of the time-varying magnetic field generated (see figures 14(a)–(iii) and (a)–(v)). The induced electric field caused by displacement of the domain walls (stray fields) as shown in figures 14(a)–(iv) and (a)–(vi), which is the cause of neurostimulation. Assuming the induced electric field has a circular contour of same width as that of the domain wall:

$$2\pi rE = -\frac{\Delta B}{\Delta t}\pi r^2 \tag{8}$$

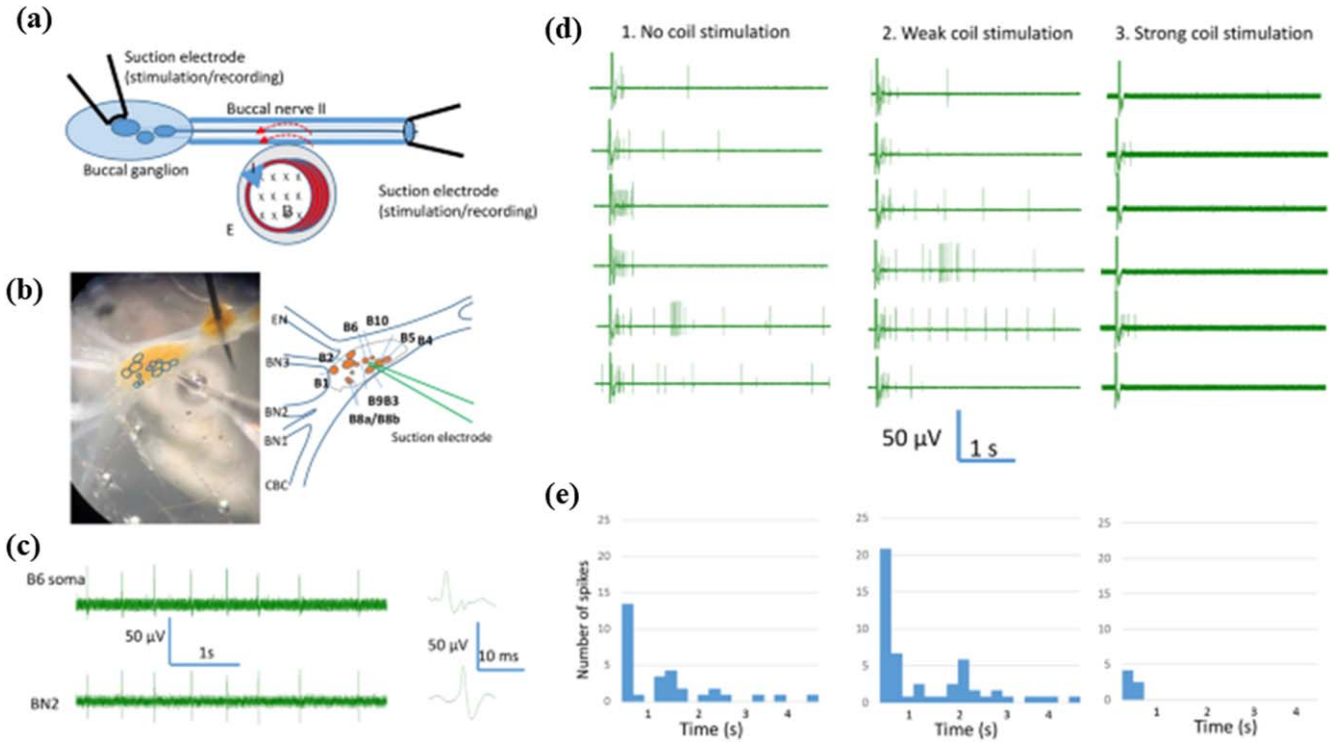

Figure 13. Commercial μcoils suppress action potentials generated by extracellular B6 soma stimulation (a) The μcoil was situated near the BN2 such that the induced electric field is generated parallel to the axon. Soma was stimulated by the electrode at B6 soma in a partially desheathed buccal ganglion. (b) Morphological location of the B6 neuron on the caudal surface of the buccal ganglion with its schematic drawn on the right. (c) Electrophysiological recordings from the B6 neuron (soma activity) showed in a one-to-one relationship with the axon activity. (d) Action potentials were triggered in the B6 soma with electric pulses (0.1 ms width, 4 s interval) through the μcoils. Axonal recordings when 1. no magnetic stimulation was applied to the BN2. 2. a weak magnetic stimulation was applied to BN2. 3. a strong magnetic stimulation was applied to BN2. (e) Histogram of the firing frequency of the six repetitions shown in (d). Reproduced from [105]. CC BY 4.0.

which gives

$$E = -\frac{r}{2}\frac{\Delta B}{\Delta t}, \tag{9}$$

where, $\boldsymbol{E}$ is the induced electric field, $\boldsymbol{B}$ is the magnetic flux density from the stray field, r is half of the total width of the domain wall and Δt is the time for one domain wall to pass the observation point. Therefore, if v is the velocity of the domain wall motion, it can be represented as $v = r/\Delta t$. Replacing this in equation (9), we obtain,

$$E = -\frac{v}{2}\Delta B. \tag{10}$$

Equation (10) specifies that the induced electric field is directly proportional to the change of the stray field and the velocity of domain wall propagation. This signifies that the induced electric field is dependent on the duration and intensity of the applied current density [129].

4.2. Skyrmion-based neursotimulator (SkyNS)

Skyrmions were experimentally observed for the first time in 2009 [130]. Since then, they have been believed to be potential candidates for next generation neuromorphic computing, ultra-fast data processors and high storage memory devices [131–133]. The dynamics of skyrmions along a heavy metal (HM)/ferromagnetic metal (FM) racetrack, with or without defects, have also been studied by several groups [134, 135]. A HM/FM nanotrack inspired from the simulation study by Huang *et al* [131] for magnetic skyrmion-based synapses is an excellent candidate for neurostimulators. Saha *et al* [127] used Mumax3 [96] to simulate in figures 14(b)–(i), a HM/FM bilayer thin film with a PMA FM layer of dimensions 500 nm × 200 nm × 1 nm with a high anisotropy barrier of dimension 80 nm × 40 nm situated at the center is mounted at the tip of a needle. The skyrmions are nucleated on one side of the barrier. On applying a charge current of the order of $\sim 10^{10}$ A m^{-2} through the HM, due to spin Hall effect (SHE), the skyrmions bypass the barrier and arrive on the other side of the barrier. The higher anisotropy barrier here acts as a hurdle in the path of the skyrmions thereby impeding the motion of the skyrmions. For neurostimulation, perfect nucleation and smooth movement of the skyrmions from one side of the barrier to the other side is desired. This is desired such that the out-of-plane magnetization component (M_z) shows a change with respect to time (see figures 14(b)–(ii)). As per Faraday's law, this will induce an electric field suitable for neurostimulation (see figures 14(a)–(iii)).

The neurostimulation performance will be dependent on the skyrmion dynamics. The velocity of the skyrmions have been reported to be controlled by, introduction of defects [131, 136], the applied current density [131, 133], the

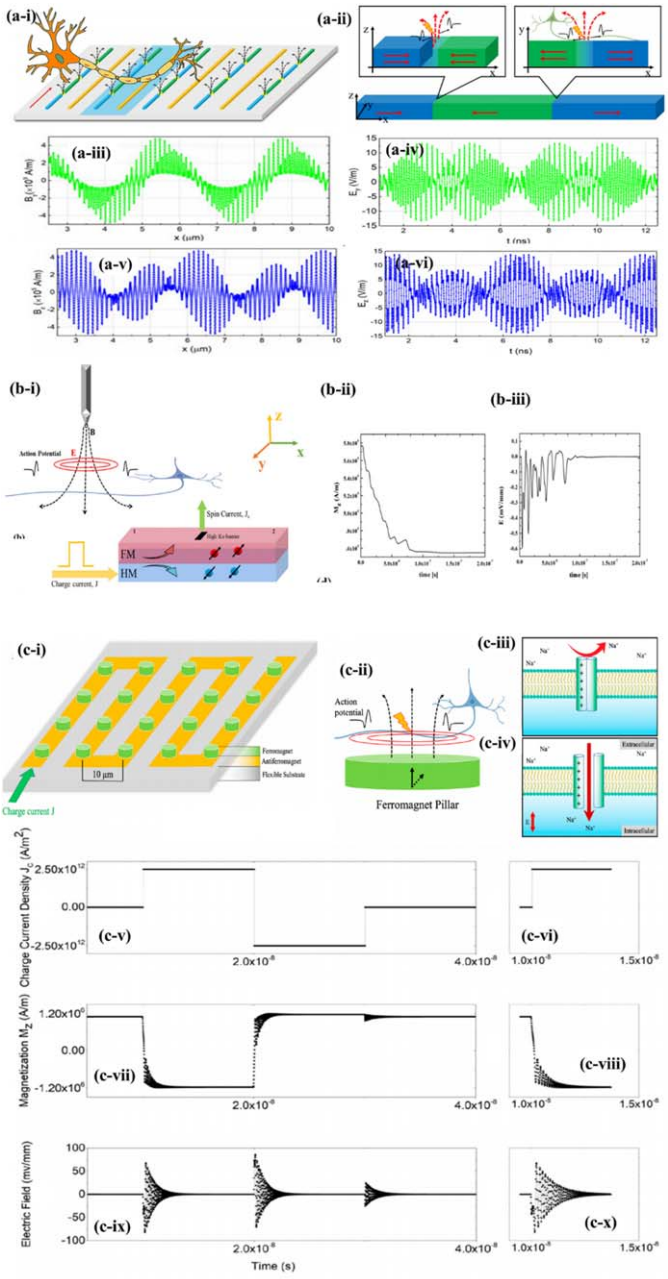

Figure 14. (a-1) Schematic illustration of the magnetic nanowire-based neurostimulator (MNNS) where different parts of the neuron can be stimulated by domain-wall movements through multiple magnetic nanowires. (a-ii) Schematic view of the domain wall movement within the magnetic nanostructure with perpendicular transverse wall (left inset) and transverse wall (right inset). The dotted red arrows represent the magnetization in that domain. (a-iii) *y*-component of the magnetic field (B_y) projected along *x*-direction. (a-iv) *y*-component of the induced electric field (E_y) obtained by applying Faraday's laws of electromagnetic induction on B_y. (a-v) *z*-component of the magnetic field (B_z) projected along *y*-direction. (a-vi) *z*-component of the induced electric field (E_z) obtained by applying Faraday's laws of electromagnetic induction on B_z. These B_z and E_z components are believed to stimulate neurons. Reprinted from [18], with the permission of AIP Publishing. (b-i) Schematic view of the skyrmion-based neurostimulator (skyNS) mounted at the tip of a needle for cellular-level neurostimulation. As reported by Saha *et al*, SkyNS is a heavy metal (HM)/ferromagnetic metal (FM) bilayer to which on application of a charge current along the HM layer due to spin hall effect (SHE), the skyrmions generated in the HM/FM bilayer system move from one end of the device to the other. (b-ii) The movement of skyrmions generate a time-varying out-of-plane magnetic field, M_z. (b-iii) On applying Faraday's law of electromagnetic induction to the time-varying magnetic field generated an induced electric field, E_z (right). Reproduced from [127]. © IOP Publishing Ltd. All rights reserved. (c-i) Spin orbit torque-based neurostimulator (SOTNS) arrays fabricated on a flexible substrate for therapeutic neuromodulation. SOTNS array is formed of an antiferromagnetic (AFM in yellow) and ferromagnetic (FM in green) bilayer. (c-ii) Schematic illustration of how the switching of a single FM pillar contributes to stimulation of a neurons (c-iii) and (c-iv). Since the FM pillars are of comparable dimensions (even smaller) to that of the neurons, it contributes to cellular-level stimulation of neurons. (c-v) and (c-iv) The time-varying current applied to the AFM bilayer which causes switching of the FM pillar thereby generating a time-varying magnetic field (c-vii) and (c-viii). On applying Faraday's law to this time-varying magnetic field, an induced electric field is generated (c-ix) and (c-x). Reprinted with permission from [128]. Copyright © 2019, American Chemical Society.

dimension of the barrier and nanotrack width [136] and the number of skyrmions nucleated [131]. For perfect nucleation of the skyrmions, the Dzyaloshinskii-Moriya interaction (DMI) value and the uniaxial anisotropy of the thin film are responsible which can be tuned by the thickness of the thin film and ion irradiation, respectively [137]. The aim should be to perfectly tune these properties such that the value of the induced electric field lies on the strength–duration curve (see figure 2(a)). However, one cannot deny a major disadvantage of skyrmionic devices in neurostimulation. It requires an external out-of-plane magnetic field for perfectly stable nucleation and smooth dynamics. However, several attempts have been made to alleviate this requirement such as investigation into synthetic antiferromagnetic skyrmions [138] and field-free deterministic nucleation of skyrmions [139].

4.3. Spin–orbit torque-based neurostimulator (SOTNS)

It has been observed that on passing an in-plane charge current, $\boldsymbol{J_c}$, to a heterostructure with structural inversion symmetry and consisting of a large spin–orbit interaction (SOI) material results in a spin–orbit torque (SOT). As a result of this torque, it causes the magnetization of adjacent perpendicularly magnetized ferromagnetic layer to switch direction [140]. This effect is typically observed in a non-magnet/ferromagnet (NM/FM) bilayer where the NM can be a heavy metal (HM) [141–143], an antiferromagnet (AFM) [144–146], topological insulators [147] or a Weyl semimetal [148]; basically a spin channel that generates the spin current. The in-plane spin polarized electrons accumulate at the interface of the NM/FM and exerts a Slonczewski-like torque (SLT) that causes the magnetization of the FM layer to switch. In general, a bias magnetic field is required to break the symmetry along the charge current direction, a phenomenon known in literature as the deterministic SOT switching [149].

As we are trying to stimulate neurons magnetically, it is not recommended to apply an external magnetic field to operate these spintronic devices. Hence, field-free switching of the FM layer must be studied. It can be achieved by introduction of interlayer exchange coupling [144, 145, 150], tilted or graded magnetic anisotropy [151], interplay of spin orbit and spin transfer torques [152], etc. In this case, the FM nanopillars on an AFM racetrack can be fabricated on to flexible substrates as in figures 14(c)–(i). On application of a current through the AFM layer (represented in yellow), it causes switching of the ferromagnetic nanopillar (represented in green). On changing the direction of the current, it causes the FM layer to switch in a different direction (see figures 14(c)–(ii)). This attributes to the tunable neurostimulation property of SOTNS in cellular level neurostimulation (see figures 14(c-iii) and (c-iv)). On application of the current through the AFM layers (see figures 14(c-v) and (c-vi)), the switching of the FM nanopillar will cause a rate of change of magnetization (see figures 14(c-vii) and (c-viii)) which will induce an electric field suitable for neurostimulation (see figures 14(c-ix) and (c-x)). The AFM layer supplies the bias field by exchange coupling and supports field-free switching of the ferromagnetic nanopillar. The applied current density must be greater than or equal to a critical current density (J_{crit}) for successful switching of the FM layer [153, 154] and therefore mediate neuromodulation. For neurostimulation purposes, we will consider only the switching of the z-component of magnetization as the FM layer has perpendicularly magnetized anisotropy (PMA). This switching can be experimentally measured by the magneto-optic Kerr effect (MOKE) signal. Also, micromagnetic simulations can give a rough estimate about the strength and duration of the induced electric field. The switching speed depends upon the thickness of the FM and AFM layer and the diameter of the FM nanopillar.

4.4. Potential applications of spintronic neurostimulators

Implantable micromagnetic stimulation (μMS) of neurons using spintronic nanodevices is a nascent concept, with theoretical studies reported so far and no experimental demonstration. It has been found that high frequency (140 Hz) electrical stimulation of hippocampal slices induces an increase in extracellular K^+ concentration and blocks neuron depolarization [155]. This finding was confirmed by Bikson *et al* [156], where at high frequency, the increased extracellular K^+ concentration led to inactivation of voltage-gated ion channels. Furthermore, the efficiency of the magnetic field is such that it can enhance adult neural stem cell and trigger cell proliferation [157]. Low intensity, high frequency repetitive transcranial magnetic stimulation (rTMS) for rehabilitation of ischemic injury or demyelination has been reported to activate microglia [158, 159], while high intensity, high frequency rTMS applied to spinal cord injury decreased microglial activation [160]. Yet, in another report, high intensity, low frequency rTMS did not significantly change microglial number in the motor cortex or hippocampus of healthy rats [161]. The significant variation in results and limited number of studies on the effects of magnetic stimulation suggests the need for deeper investigation into this area which opens a plethora of opportunities for research.

The spintronic neurostimulators discussed herein show a high frequency of operation, *i.e.* they generate nanosecond pulsed electric field (nsPEF) for stimulation (see figures 14 a (iv) and (v)) for MNNS, figure 14 (b-iii) for SkyNS, figures 14(c-ix) and (x) for SOTNS. This domain of research has been under the spotlight for almost a decade now [162, 163]. Although most applications for nsPEF have been found to be extremely efficient in tumor ablation and cancer therapies (see figure 15(a)) [164, 165], there are several controversial views in terms of neurostimulation. Some reports suggest that nsPEF inhibits action potential in primary hippocampal neurons [162] while several groups have recently reported the focal stimulation efficiency of nsPEF on neurons [166–168]. Romanenko *et al* [168] have reported the generation of action potentials from a single pulse of 10 ns. Casciola *et al* [167] reported activation of a peripheral nervous system by a 12 ns stimuli and Pakhomov *et al* [166] reported neuronal membrane excitation by a 200 nsPEF. All these nsPEF stimulation methods involve extremely complex

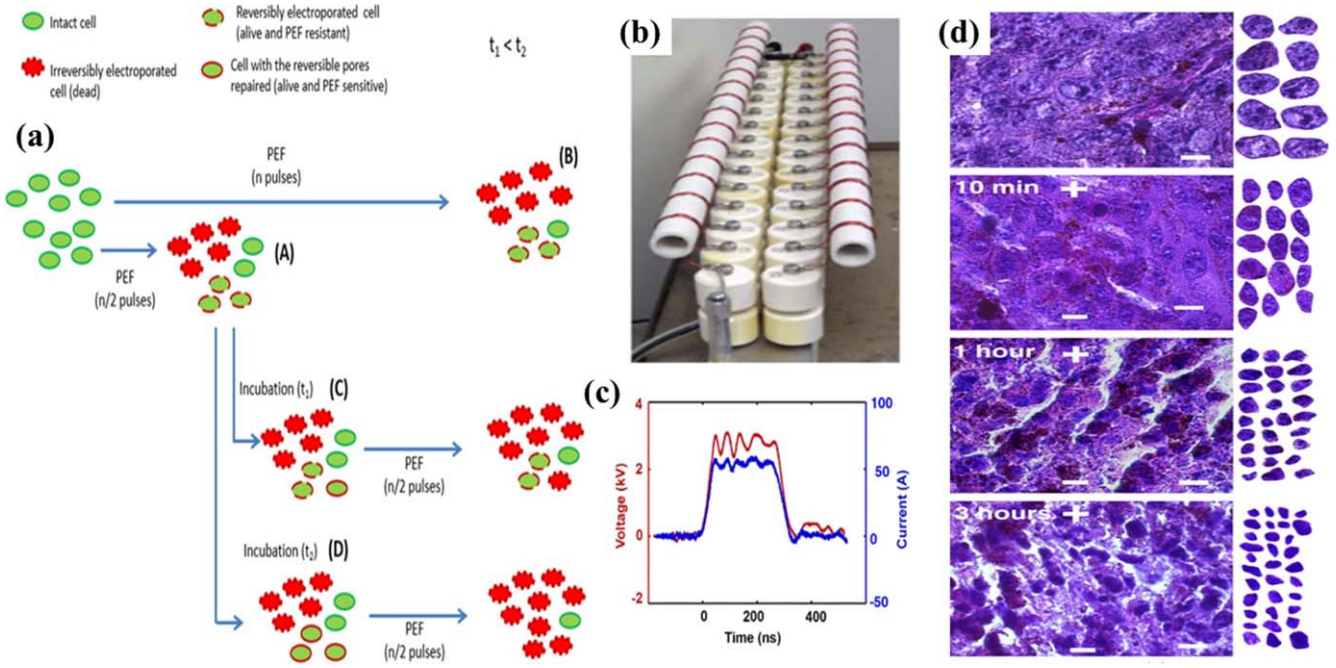

Figure 15. (a) General response of cells to an externally applied nsPEFs of different intensity, duration and number of pulses (*n*). Reprinted from [164], © 2020 Elsevier B.V. All rights reserved. (b) nsPEF generator [165]. (c) nsPEF from the experimental set-up in (b) [165]. (d) Demonstration of the fragmentation of the stained nuclei of the tumor cells for varied duration of application of the nsPEF in (c). Reprinted from [165], Copyright © 2006 Elsevier Inc. All rights reserved.

pulse generator hardware (see figures 15(b) and (c)). Even though the molecular mechanism associated with nsPEF neurostimulation is still unclear, promising experimental reports from several groups in the field of nsPEF-based tumor therapy validate the potential of the spintronic neurostimulators as a futuristic low-power implantable nanosecond pulsed electric field neurostimulator.

In this section 4, we have discussed the working principles for 3 different kinds of spintronic nanodevices, namely, SkyNS, SOTNS and MNNS. However, all 3 of them are theoretical works so far. Preliminary experiments on spintronic nanodevices have its own challenges. Usually, demonstration of a new neurostimulation implant follows a specific experimental flowchart. First, there is *in vitro* demonstration of its neuron activation performance followed by its *in vivo* demonstration. Traditional *in vitro* performance demonstration using brain slices on these spintronic nanodevices might be challenging because of the very fast attenuating stray fields [128]. However, *in vitro* demonstration is possible by culturing neuron cells directly on the surface of these spintronic devices. This could pave the way for experimental study on cellular-level neurostimulation. However, such kind of cellular-level study needs extensive troubleshooting of the biocompatibility of the encapsulation coating of the device surfaces. For *in vivo* performance demonstration, one needs to fabricate the spintronic nanodevices at the tip of a pencil-shaped structure such that they can be inserted deep into the brain. Probably, designing the mechanical design is the challenging part. Although for spintronic nanodevices, implant biocompatibility is not a significant concern. This is because nowadays, almost any device fabricated on silicon substrates can be encapsulated with a coating of the Parylene-C polymer. However, Parylene-C does not adhere too well with some thin film interfaces. In that case, we need silane A-174 adhesion promoter for better adhering the Parylene-C to most thin film interfaces [169]. There might be another potential concern for experimental demonstration of spintronic nanodevices in terms of the defects and edge roughness necessary for generation for skyrmionics and domain wall dynamics [170]. This could cause potential Young's modulus mismatch between the spintronic implants, MNNS and SkyNS, and the brain tissue causing more tissue damage than necessary. Probably there is a lot of concerns to address before experimentally diving into employing spintronic nanodevices as neurostimulation implants. However, the potential of these spintronic neuroimplants to selectively stimulate at a cellular-level and targeted treatment of tumor cells make giving their experimental demonstration worth a try.

5. Magnetic nanoparticles (MNPs) in neurostimulation

Although the current stage micro-/nano-electrodes technology is mature enough to provide reliable neurostimulations, the chronic stability and biocompatibility of devices require further validation before translating to clinical settings [171]. For instance, neurostimulation electrodes that actively inject charge currents have not yet reliably demonstrated continuous function in the body for ten years or more, which is a recognized indicator of clinical feasibility. On the other hand,

magnetic nanoparticle (MNP)-based remote neurostimulation with high spatiotemporal resolution and specificity is one class of invaluable neurotechnology that emerged in recent years [172, 173]. Combined with externally applied magnetic fields, MNPs offer several capabilities for neurostimulation that are not available in conventional brain stimulation techniques. Firstly, MNPs can interface with the nervous system at cellular and even molecular levels due to their nanometer-scale sizes. Secondly, some unique properties such as magnetic hyperthermia and magnetoelectric can be triggered and controlled remotely by means of applying magnetic fields [20, 174]. Thirdly, the free-standing MNPs face less problems with the biocompatibility and neuro-interfacing issues. Benefiting from the facial synthesis and surface functionalization of MNPs [175–177]. In addition, it overcomes the physical limitations of other neurostimulation techniques such as invasive surgical implants. Thus, allowing for pharmacological interrogation of targeted neural populations in freely moving subjects [19].

5.1. Magnetothermal neurostimulation

The temperature fluctuations can cause a perturbation of neuronal activity either through the plasma membrane or the temperature-sensitive membrane proteins. Many researchers have reported that spatially localized temperature gradients on neuronal tissues can increase the membrane capacitance and trigger action potential [174, 178–181]. Slow and prolonged heating can also inhibit the normal neural activity and suppress the epileptiform activity [182]. Optical stimulations with Au (gold) nanoparticles are prevalently used for this purpose while, this technique is limited by the inability of visible light to penetrate deep into tissues [183–185]. On the other hand, the low radiofrequency magnetic fields can penetrate into the body without substantial attenuation and allow the precisely controlled remote neurostimulation with the MNPs [186–188]. In addition, compared to the implanted electrodes for DBS, the MNP-based thermal neurostimulation is less invasive and the stimulation can be wirelessly controlled by externally applying magnetic fields. The magnetothermal neurostimulation is achieved through the activation of the heat-sensitive transient receptor potential cation channel subfamily V member 1 (TRPV1), also known as the capsaicin receptor and the vanilloid receptor 1, as shown in figure 16(a) and (b) [174, 189–191]. Magnetothermal is achieved by MNPs dissipating heat via the hysteresis loss when subjected to alternating magnetic fields (AMFs) [192, 193]. Same to the magnetic hyperthermia which has long been applied for the cancer treatment [192, 194–196]. Herein, we will give one example of magnetothermal modulation of neural activities through the hyperthermia of MNPs.

Mushi *et al* reported the wireless deep brain magnetothermal stimulation that can sufficiently evoke the motor behavior in awake, freely moving mice [188]. To avoid the heat loss to the surrounding buffer fluid from MNPs, they used membrane-targeted MNPs that can directly bound to cell membrane of temperature-sensitive $TRPV1^+$ channels and effectively deliver power to raise the temperature and evoke motor behaviors of mice. In this way, they have successfully activated three separate brain regions: motor cortex, dorsal striatum and the ridge between dorsal and ventral striatum. As shown in figure 16(d), the MNPs with 8 nm Co-ferrite core and 2.25 nm Mn-ferrite shell are synthesized and coated with 5.4 nm Poly(methyl acrylate) (PMA) for better colloidal stability. These MNPs are superparamagnetic and show a specific loss in power (SLP) of 733.3 $\pm$ 2.8 W g^{-1} at 37 kA m^{-1} and 412.5 kHz. To target these MNPs specifically to the cell membrane and meanwhile using fluorophores to monitor the temperature in molecular scale. MNPs are surface functionalized with antibodies against endogenous neuronal surface markers and fluorescent protein tags. As shown in figure 16(e), fluorescent micrographs of GCaMP6f + neuron (green) is successfully labeled with MNPs (red). The local temperature rise by MNPs can be estimated from the fluorescence intensity of fluorophores as shown in figures 16(c) and (f).

The responses of $TRPV1^+$ hippocampal neurons to magnetothermal stimulation are firstly examined by investigating the spontaneous firing rate of 10 day old $TRPV1^+$ and $TRPV1^-$ (control neurons, without TRPV1) neurons across a range of bath temperatures from 32 to 39 °C, as shown in figure 16(g). With the increase of bath temperature, the action potentials (APs) increase from 1.5 $\pm$ 1.2 per 5 s to 13 $\pm$ 3 in the same period. While for the control neurons, a slight decrease of spiking rate to 1 $\pm$ 1 APs per 5 s is observed. Thus, confirming that the TRPV1 in hippocampal neurons renders their firing rate highly heat-sensitive without disrupting natural function. Then the hippocampal neurons with TRPV1 are bound with MNPs as is confirmed from the fluorescence signals in figure 16(e). With the application of AMF at 22.4 kA m^{-1} and 412.5 kHz for 5 s, an increased spiking measured by $Ca2^+$ transients are observed from $TRPV1^+$ neurons, as shown in figure 16(h). During the AMF application, the neuron membrane temperature is measured by the fluorescence signal and showed an increase of 2 °C in figure 16(i), which caused the spiking increasing from basal activity (1.8 $\pm$ 0.6 APs) to 12.1 $\pm$ 2.0 APs in the 5 s AMF window, then to 4.5 $\pm$ 1.2 APs after the removal of AMF, as shown in figure 16(j).

Then these MNPs are applied to stimulate the motor cortex neurons to evoke precise behavior in an awake, moving mouse. A total of 6 mice in 14 trials running along the periphery of the arena are monitored as shown in figure 16(k). To illustrate the contrast between the induced and the resting behaviors, the track of the head of a representative mouse is shown in figure 16(l). The monitored running path along the periphery of the circular arena recorded during the AMF field is in sharp contrast to the resting status (before and after the AMF field), as shown in figure 16(m). The detailed data in figure 16(n) shows that upon the application of AMF, the mouse initiated running, which slowed down quickly after the removal of AMF. Repeat stimulation of the same animal evoked increased movement reliably in each trial. The linear running speed and angular speed of one mouse in 4 trails are summarized in

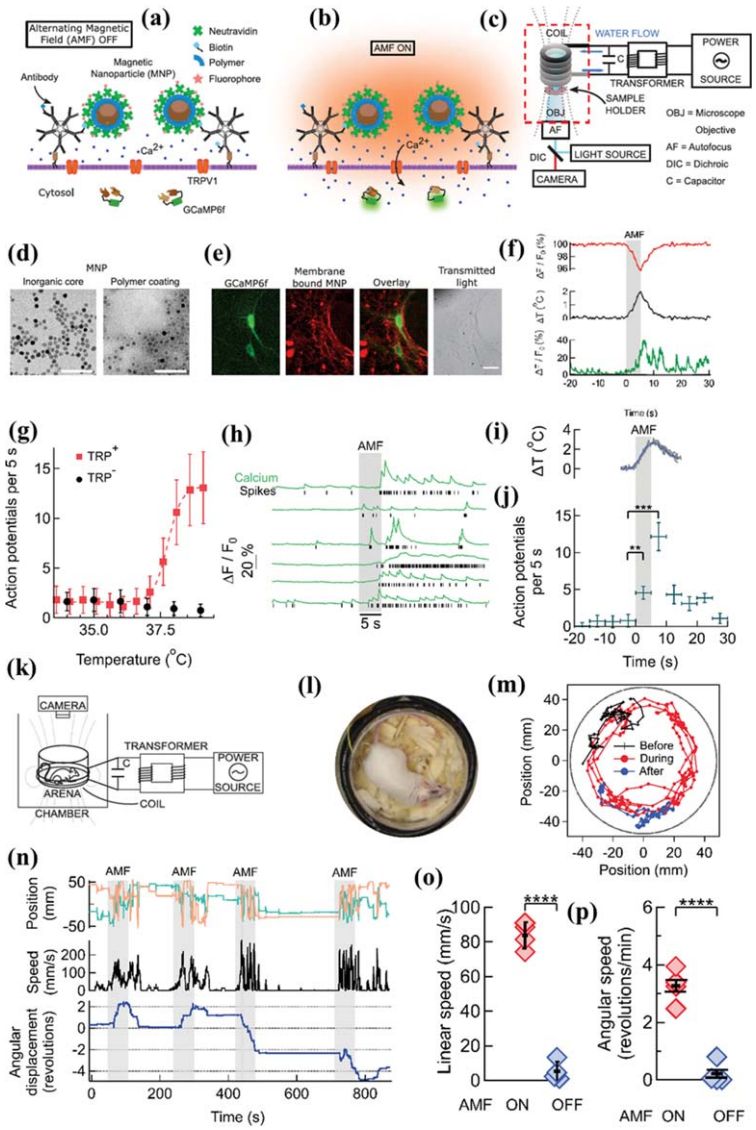

Figure 16. Magnetothermal neurostimulation activates the TPRV1 channels by heating membrane bound MNPs using an AMF. (a) MNPs encapsulated in PMA polymer are functionalized with NeutrAvidin conjugated with Dylight550 fluorophores, then bound to the neuronal membrane via biotinylated antibodies targeting membrane proteins. The neurons are transfected to express temperature sensitive TRVP1 channels and the calcium indicator GCaMP6f. (b) Applying an AMF heats the MNPs bound on neural membrane and rises the temperature locally, which activates the TRPV1 channels. The resulting Ca^{2+} influx depolarizes the neurons and is measured as a transient intensity increase of the GCaMP6f fluorescence. (c) The experimental setup combining the AMF application with fluorescence microscopy for *in vitro* studies. (d) TEM images of core-shell MNPs as synthesized (left) and PMA polymer shell coated MNPs (right). Scale bar represents 100 nm. (e) From left to right: fluorescent micrographs of GCaMP6f + (green) neuron; membrane bound MNPs (red); overlay of the GCaMP6f (green) and MNP (red) signals; and transmitted light image of the same neurons. Scale bar represents 10 mm. (f) (Top) Local heating of MNPs during AMF application measured as a dip in DyLight550 fluorescence intensity, which drops linearly with increasing temperature. The grey bar indicates the application of the AMF. (Middle) Calculated temperature change near MNPs. (Bottom) The GCaMP6f fluorescence signal recorded in the neuron decorated with MNPs shows a Calcium transient after 5 s of AMF when the membrane temperature increased by 2 °C. Temperature decreased after the AMF was removed and the Calcium transients slowly subsided again. (g) Within seconds of AMF application, membrane targeted MNP stimulate magneto-thermally $TPRV1^{+}$ neurons in culture. Rate of action potential (AP) firing as a function of bath temperature, recorded from GCaMP6f transients observed in TRPV1 expressing hippocampal neurons (red) and wild-type neurons (control, black) when perfused with pre-heated buffer. The Ca^{2+} transients are modeled by a spike train. (h) GCaMP6f fluorescence intensity changes (green, Ca^{2+}) in different $TPRV1^{+}$ neurons decorated with MNP (5 s field, 22.4 kA m^{-1} at 412.5 kHz, in gray). Calculated spike events (black) are indicated under each Ca^{2+} trace. (i) Change of cell surface temperature estimated from DyLight550 fluorescence intensity. (j) GCaMP6f signal recorded from MNP bound $TRPV1^{+}$ neurons in 5 s intervals. (k) Experimental set-up for *in vivo* magnetothermal stimulation of motor behavior in awake mice. A water-cooled two-turn coil around the arena generated the AMF. An overhead camera was used to record the mouse's behavior in the arena. (l) Photograph of mouse in the observation arena. (M) Representative trajectory recorded from a mouse stimulated in the motor cortex before (black), during (red), and after (blue) AMF application. (n) (Top) Position of the mouse's head, (*x* green; *y* orange) measured taking the center of the arena to be the origin. (Middle) Black trace shows the linear speeds of the mouse. Speed markedly increases during all AMF applications (Grey bars). (Bottom) After each AMF application, the mouse slows down regular exploratory motion. Comparison of (o) linear and (p) angular speed of this mouse with MNPs injected in the motor cortex, with and without AMF. Reproduced from [188]. CC BY 4.0.

figures 16(o) and (p) where significant differences are observed with AMF on and off.

Overall, this MNP-based magnetothermal stimulation offers genetically and spatially targetable, repeatable, and temporarily precise activation of deep brain circuits without the need of surgical implantations of electrodes. Although this method has shown many advantages over the optical stimulation and is less invasive compared to the implanted electrodes. The concern of thermal tissue damage caused by MNP heating should not be ignored [187, 197]. The magnetothermal control of neural activities requires more in-depth studies before reaching to clinical stage.

In addition, some pharmacological neuromodulation using MNPs loaded with drugs and the hyperthermia of MNPs to release drugs at target neurons is also another method that have been extensively reported [19, 186, 198]. However, this method is categorized as pharmacological neurostimulation since the heat generated by MNPs is not the direct reason of neurostimulation. The only function of magnetic hyperthermia is to trigger the release of loaded drugs.

5.2. Magnetomechanical neurostimulation

Like the magnetothermal neurostimulation strategy that uses heat to trigger the heat-sensitive ion channels, the magnetomechanical neurostimulation uses mechanical forces to trigger the mechano-sensitive ion channels. Transient receptor potential cation channel subfamily V member 4 (TRPV4) is an ion channel protein that reported to be responsive to mechanical forces [199, 200]. Wheeler *et al* firstly explored the possibility to use the magnetic forces from MNPs to trigger the Ca^{2+} influx by opening the TRPV4 ion channels [201]. Later Tay *et al* identified that N-type mechano-sensitive Ca^{2+} ion channel plays a key role in response to the magnetic force [202]. They used starch-coated MNPs that can bound to the neural membrane instead of being internalized. Upon the application of magnetic fields, the magnetomechanical stimulation triggers the Ca^{2+} influx in neurons. They demonstrated that the magnetic forces could enhance the open probability of the ion channels and facilitate the Ca^{2+} influx. However, it should also be noted that there might be other unknown mechano-sensitive ion channels contributing to the Ca^{2+} influx such as PIEZO1 and NMDA receptors [203, 204]. In this work, the authors reasoned that it is most likely the magnetically induced Ca^{2+} influx is due to the N-type Ca^{2+} channels. They also applied this method for chronic stimulation of a fragile X syndrome (FXS) neural network model and found that magnetic force-based stimulation modulated the expression of mechano-sensitive ion channels which are out of equilibrium in a number of neurological diseases including FXS.

In addition to MNPs, Gregurec *et al* synthesized magnetic nanodiscs (MNDs) with diameters of 98–226 nm and thickness between 24 and 37 nm for remote control of mechanosesory neurons [21]. They demonstrated these MNDs can serve as versatile transducers to remotely trigger Ca^{2+} influx in week and slowly varying magnetic fields (<28 mT, <5 Hz). Figure 17(a) shows the SEM images of synthesized MNDs with controllable sizes. They adapted a high-throughput protocol that relies on a solvothermal synthesis of hematite (α-Fe_2O_3) nanodiscs with a hexagonal lattice, followed by the reduction into magnetite MNDs (figure 17(a: i)). By tuning the amount of water in the solution, they can synthesis hematite MNDs with average sizes from 226 nm down to 98 nm. The magnetic vortex states of 226 nm, 181 nm, and 98 nm MNDs are characterized by electron holography as shown in figure 17(b: i–iii). These particles show zero net magnetizations with negligible demagnetization fields. The magnetization field in each particle, as shown in figure 17(b: iv–vi), can reach to 0.6 T locally, corresponding to a saturation magnetization of 128 $Am^2\ kg_{Fe}^{-1}$.

It is hypothesized that the transition of magnetization states of MNDs under the magnetic fields can exert torques mimicking the biological mechanotransduction as shown in figure 17(c). And this torque is proportional to the magnetic moments of MNDs. The effect of MND caused stimulation is firstly proved on cultures of dorsal root ganglia explants (DRGs). DRGs contain sensory neurons expressing a wide range of mechanoreceptors. As mechanotransduction in sensory neurons involves changes in membrane potential and Ca^{2+} influx, the effects of magnetically mediated torques on the cells decorated with MNDs can be monitored via the fluorescence change of the Ca^{2+} indicator: Fluo-4. The Ca^{2+} imaging of DRGs incubated with MNDs (either 98 or 226 nm) are carried out under varying magnetic field amplitudes and frequencies as shown in figure 17(d). The results confirm that the highest frequencies and amplitudes resulted in the highest percentages of responding cells.

To further explore whether the neuronal activation caused by the MND torque is mediated by mechanosensitive ion channels, they inhibited two major mechanoreceptors present in DRGs: the PIEZO2 and TRPV4. Each receptor is inhibited by incubating DRG neurons with GsMTx4 and HC-067047, respectively. Results in figure 17(e) show that after the first magnetic field plus, there is a decrease in neuron activity. Thus, individually inhibiting mechanosensitive channels significantly reduces the efficacy of magnetomechanical stimulation. The possibility of voltage- or ligand-gated channels in DRGs contributing to the magnetomechanical stimulation is also excluded by testing the non-mechanosensitive cells, human embryonic kidney (HEK-293), as shown in figure 17(f). This preliminary work demonstrated that switching the magnetizations in MNDs can transduce local torques that could be used for triggering mechanoreceptive sensory neurons in the presence of slowly varying magnetic fields.

5.3. Magnetoelectrical neurostimulation

In this section, we will introduce another type of MNP-based neurostimulation method that also relies on the control of wireless magnetic field but uses the magnetoelectric (ME) nanomaterials. Similar to the inductive coils, the ME nanomaterials transform a magnetic field to an electric field [20, 205, 206]. To be specific, the application of magnetic

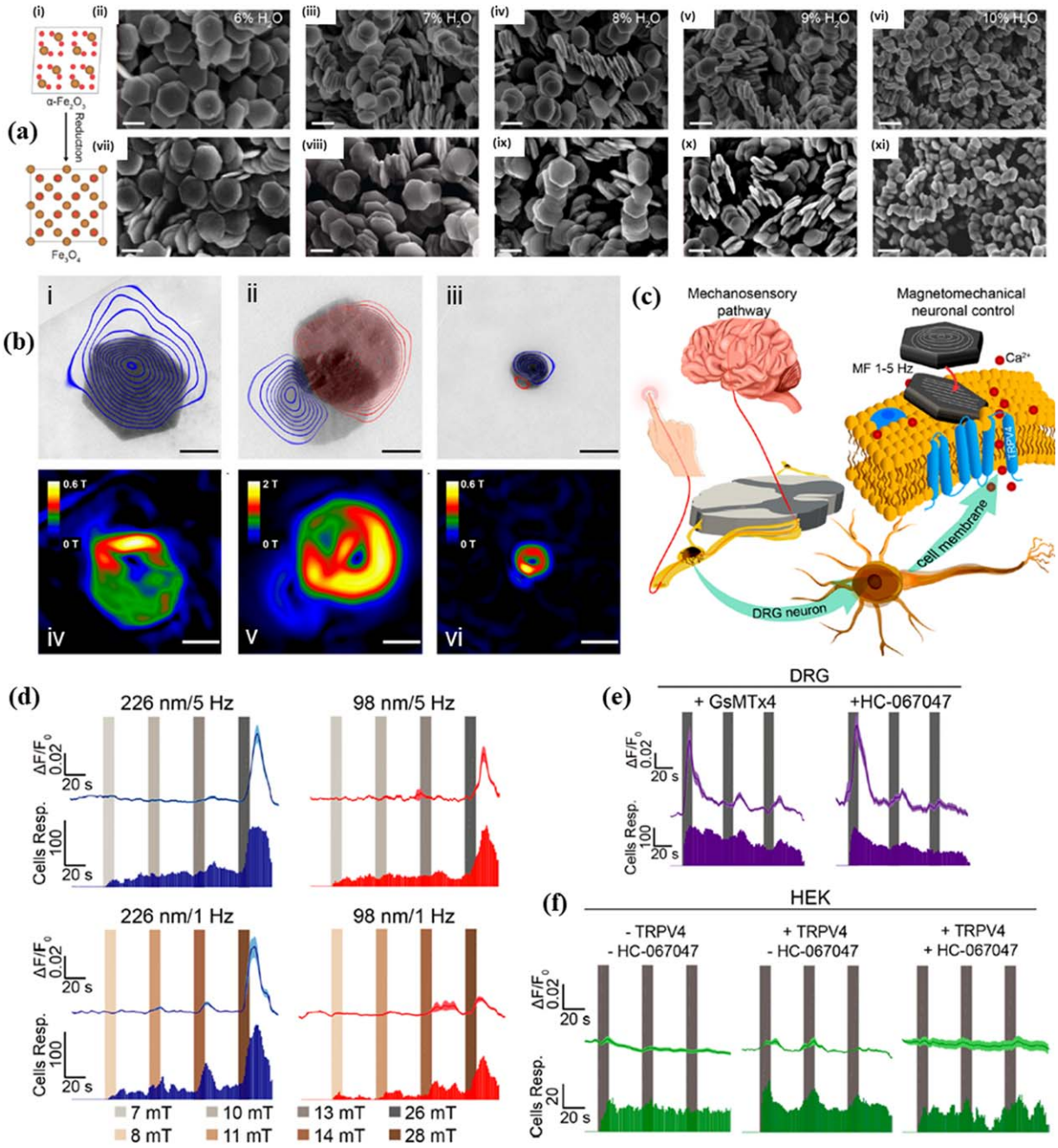

Figure 17. (a) Synthesis of MNDs. (i) Crystal units of nonmagnetic hematite phase converted to magnetic magnetite after reduction. SEM images of nanodiscs synthesized in a two-step solvothermal reaction with 6% H_2O (ii, vii), 7% H_2O (iii, viii), 8% H_2O (iv, ix), 9% H_2O (v, x), and 10% H_2O (vi, xi). (ii−viii) and (vii–xi) are the hematite (α-Fe_2O_3) and magnetite (Fe_3O_4) nanodiscs. Scale bars are 200 nm. (b) (i −iii) Electron holographs of MNDs: magnetic field lines overlapping the MNDs with 226, 181, and 98 nm in diameter, respectively. Blue and red lines denote vortices of opposite directions. (iv–vi) Correspond to magnetizations of upper images. Scale bars are 100 nm. (c) Magnetomechanical stimulation of MND-decorated DRG neurons allows for remote activation of Ca^{2+} influx. DRGs relay sensory information, including mechanosensory information, to the spinal cord. DRG explants incubated with MNDs can be stimulated when slowly varying magnetic fields that cause the magnetizations of MNDs to transform from vortex to in-plane. Thus, producing magnetic forces on mechanosensitive ion channels and resulting in Ca^{2+} influx. (d) Tuning parameters for magnetomechanical stimulation in DRG neurons and demonstration of magnetomechanical stimulation in HEK-293 cells transfected with TRPV4. Fluorescence traces resulting from stimulation of DRG neurons incubated with 226 nm (left) and 98 nm diameter MNDs (right) with magnetic field amplitudes and frequencies varied. Magnetic field is applied in 4 pulses of 10 s with 30 s wait times between pulses. (e) DRGs incubated with 1 μM PIEZO2 inhibitor GsMTx4 (left) and with TRPV4 inhibitor HC-067047 (right) both show a decrease in activity after the first stimulation sequence. (f) The response of unmodified HEK-293 cells decorated with MNDs to magnetic field (left), the response of HEK-293 cells expressing TRPV4 decorated with MNDs to the magnetic field (middle), and the blocked response of HEK-293 cells decorated with MNDs, expressing TRPV4, and incubated 1 μM TRPV4 inhibitor HC-067047 (right). Reprinted with permission from [21]. Copyright © 2020, American Chemical Society

field causes strain in the magnetic cores and thus, created a charge separation (see figure 18(a)) in ME nanomaterials that can directly interact with the neural network for localized and targeted brain stimulation.

For example, Kozielski *et al* demonstrated the application of magnetoelectric nanoparticles (MENPs) for both *in vivo* and *in vitro* neuronal modulations [206]. As shown in figures 18(a) and (b), MENPs composed of magnetostrictive $CoFe_2O_4$ cores and piezoelectric $BaTiO_3$ shells are synthesized. The morphologies and magnetostrictive to piezoelectric material ratio of MENPs are characterized by TEM and TEM-EELS as shown in figures 18(d) and (e), respectively. To maximize the ME output (also called ME coefficient) of these MENPs, AC magnetic field with a large DC bias is applied along the same axis to align the magnetic domains, axis of magnetostriction, and piezoelectric poling axis as shown in figures 18(b). The calculated ME coefficient of these MENPs is 86 V m^{-1} T^{-1} at 200 and 225 mT. Furthermore, the ME coefficient shows little dependence on the AC magnetic field frequency across the range of 35 to 385 Hz, which covers the range of DBS frequencies found to have clinical effect.

The ability of MENPs for magnetoelectric stimulation is firstly examined *in vitro* using intracellular Ca^{2+} signaling in human SH-SY5Y cells, as shown in figure 18(f). MENPs are administered as a suspension in the medium while for the control groups there are either no nanoparticles (NPs), or only MSNPs (magnetostrictive nanoparticles), or only PENPs (piezoelectric nanoparticles). The magnetic field parameters are either no field, a 225 mT DC field, a 6 mT, 140 Hz AC field, or both DC and AC fields. A significant increase of Ca^{2+} transients is observed when MENPs are stimulated with a simultaneous AC and DC magnetic field versus basal activity.

The *in vivo* neuromodulation is carried out by injecting the MENPs into the subthalamic area via stereotactic infusion in freely moving mouse as shown in figure 18(c). It is shown that the local c-Fo protein expression is significantly increased in the motor cortex and nonmotor thalamus following the stimulation of MENPs under an AC and DC magnetic fields compared to only DC field, as shown in figure 18(g–l). Then two groups of mice are injected with MENPs or MSNPs (control). The mice behaviors with AC and DC magnetic fields or with only DC magnetic field are recorded in a rotarod test and a CatWalk analysis system as shown in figure 18(m). The dynamic parameters of the CatWalk test indicate a significant difference in the behavior of MENP-treated mice compared with the MSNP-treated ones. To be specific, the average speed, duty cycle of each limb, and stride length of each limb all changed significantly in MENP-treated mice following AC and DC field stimulation but not in MSNP-treated mice (figure 18(n)). In addition, the gait- and balance-related static parameters such as regularity index, run maximum variation, and base of support, showed no significant difference following AC and DC stimulation in both mice groups treated with MENPs and MSNPs (figure 18(o)). Which confirms that the magnetic stimulation caused by MENPs does not affect animal motor activities.

These results demonstrate the potential of ME nanomaterials for wireless magnetoelectrical modulation of neural activities. And this modulation is sufficient to change animal behavior and to modulate other regions of the corticobasal ganglia-thalamocortical circuit.

Furthermore, the availability of novel MENPs with colossal ME coefficient values favors the better neurostimulation performance with minimal MENP dosage. Wang *et al* reported 20 nm $CoFe_2O_4$-$BaTiO_3$ and $NiFe_2O_4$-$BaTiO_3$ core-shell MENPs showing colossal magnetoelectric coefficient values of above 5 and 2 V cm^{-1} Oe^{-1}, respectively [205]. This ultra-high magnetoelectric coefficient is attributed the heterostructural lattice-matched interface between the magnetostrictive core and the piezoelectric shell. Nguyen *et al* also reported a similar core-shell MENP structure showing ME coefficient of >5 V cm^{-1} Oe^{-1} [207]. In their work, they have demonstrated the ability of using MENPs to wirelessly activate cortical neurons and cortical network *ex vivo* and *in vivo*. The *ex vivo* and *in vivo* Ca^{2+} imaging data supports that MENPs evoke cortical neuronal activity with fast temporal resolution at cellular and global network levels. Furthermore, the process of MENPs delivery and magnetic stimulation did not induce detectable neuroinflammation.

On a separate note, Singer *et al* reported the wireless ME neurostimulation that can provide therapeutic deep brain stimulation in a freely moving rodent model for Parkinson's disease (PD) [208]. Where the ME stimulator is not MENP, instead, it's a rectangular film with magnetostrictive layer bound to a piezoelectric layer, in the size of a grain of rice (<25 mm^2 in area).

6. Challenges and opportunities of micromagnetic neurostimulation

Electrical and magnetic stimulation, both have been excellent sources for neuromodulation therapies. Electrical stimulation is usually applied through electrodes in the brain while, magnetic stimulation is performed transcranially, in a non-invasive manner but not focally. In implantable micromagnetic neurostimulation (μMS), the induced electric field that is generated from a time-varying magnetic field as per Faraday's law of electromagnetic induction is spatially asymmetric. Therefore, this focal stimulation with magnetic fields may activate different populations of neurons than electrical stimulation, giving us the flexibility to study different population of neurons which are otherwise not investigated through electrical stimulation. In addition, these magnetic implants do not need to be in direct galvanic contact with the biological tissues, thereby avoiding the electrochemical interface with the brain. This prevents intense immune reaction and inflammatory response by tissues on implantation of these implants thereby significantly reducing biofouling nuances. Therefore, implantable magnetic stimulation eliminates many safety limitations in the waveforms that can be applied to drive these devices.

Figure 19(a) shows the comparison between the neural response from DBS microelectrodes and magnetic μcoils as

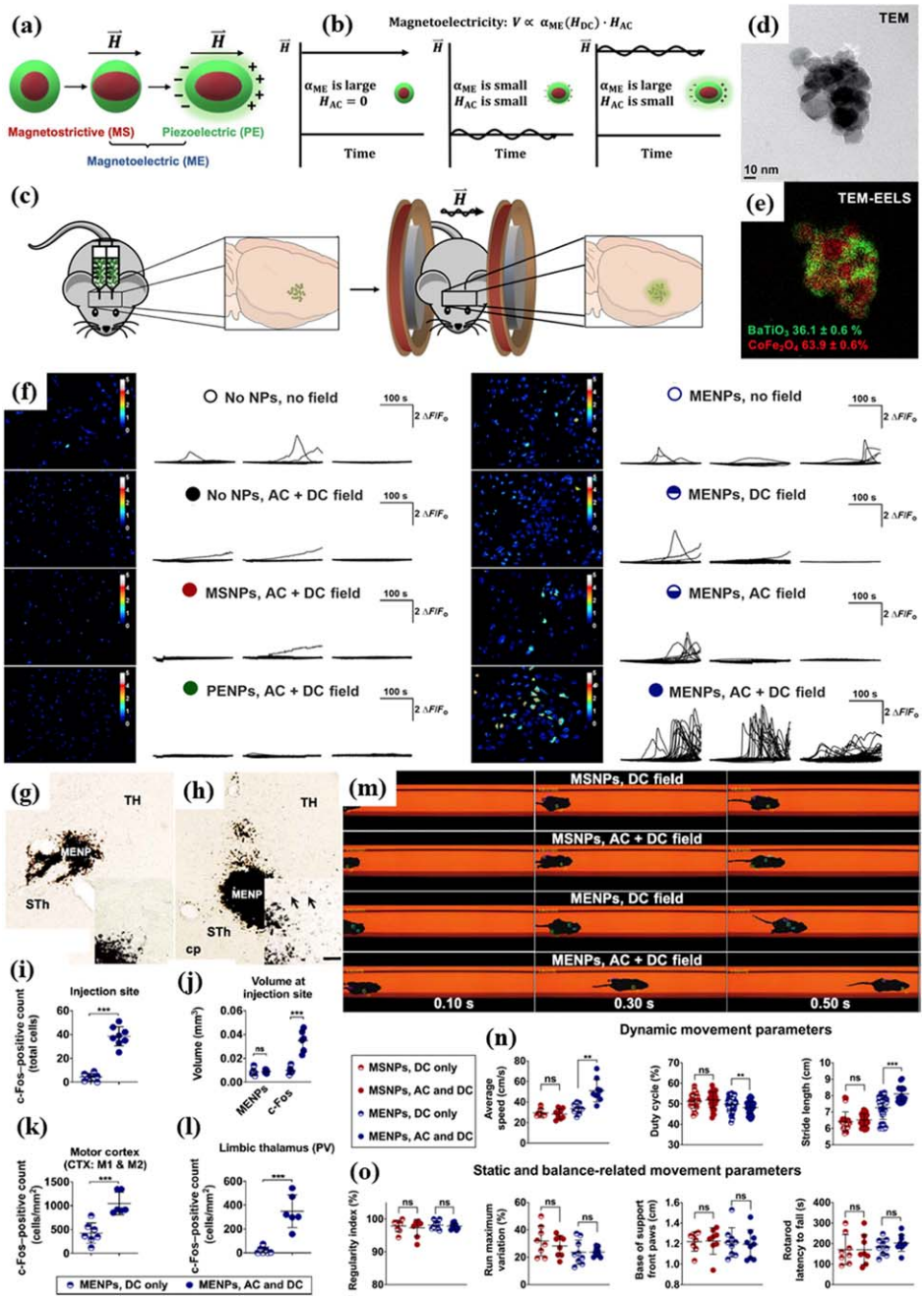

Figure 18. (a) Schematic view of one MENP consisting of magnetostrictive core and piezoelectric shell. (b) Schematic demonstrating the rationale for using a large DC magnetic field overlaid with an AC field to generate optimal magnetoelectric output. (c) MENPs are injected bilaterally into the subthalamic region of mice and are wirelessly stimulated using an AC and DC magnetic field. The (d) TEM and (e) TEM–electron energy loss spectroscopy (TEM-EELS) images show MENP morphology and $BaTiO_3/CoFe_2O_4$ phases (green and red, respectively), with quantitative elemental analysis measurement of the molar percentage of each material. (f) Magnetic stimulation of MENPs modulates neuronal cell activity *in vitro*. Cells were treated with MENPs, using no NPs, MSNPs, or PENPs as controls. Magnetic stimulation was 220 mT DC, 6 mT and 140 Hz AC, or both DC and AC fields along the same axis (AC + DC). Neuronal activity was measured via intracellular Ca^{2+} imaging using Fluo4 dye. Images of total Ca^{2+} activity over time is shown for selected experimental groups. Magnetic stimulation of MENPs locally modulates neural activity in mice, yielding modulation of basal ganglia circuitry and behavioral change. Staining for c-Fos protein locally to the MENP injection site following DC magnetic stimulation (g) or AC and DC magnetic stimulation (h) shows increased c-Fos expression (i) and increased c-Fos–positive tissue volume (j) in the latter. Quantification of c-Fos in the motor cortex (k) and limbic thalamus (l) shows increased expression when MENPs were stimulated with an AC and DC magnetic field versus only a DC magnetic field. (m) Dynamic movement parameters as measured by the CatWalk recording showed significant changes in mouse speed, limb duty cycle, and limb stride length (n) in MENP-treated mice following AC and DC stimulation versus DC stimulation, while MSNP-treated mice showed no significant change. Static movement parameters of mouse movement such as regularity index, run maximum variation, and front-paw base of support as measured by CatWalk recording did not significantly change with AC and DC versus DC only magnetic stimulation in either nanoparticle group (o). Rotarod latency to fall also did not significantly change with AC and DC versus DC only magnetic stimulation in either nanoparticle group (o). From [206]. Reprinted with permission from AAAS.

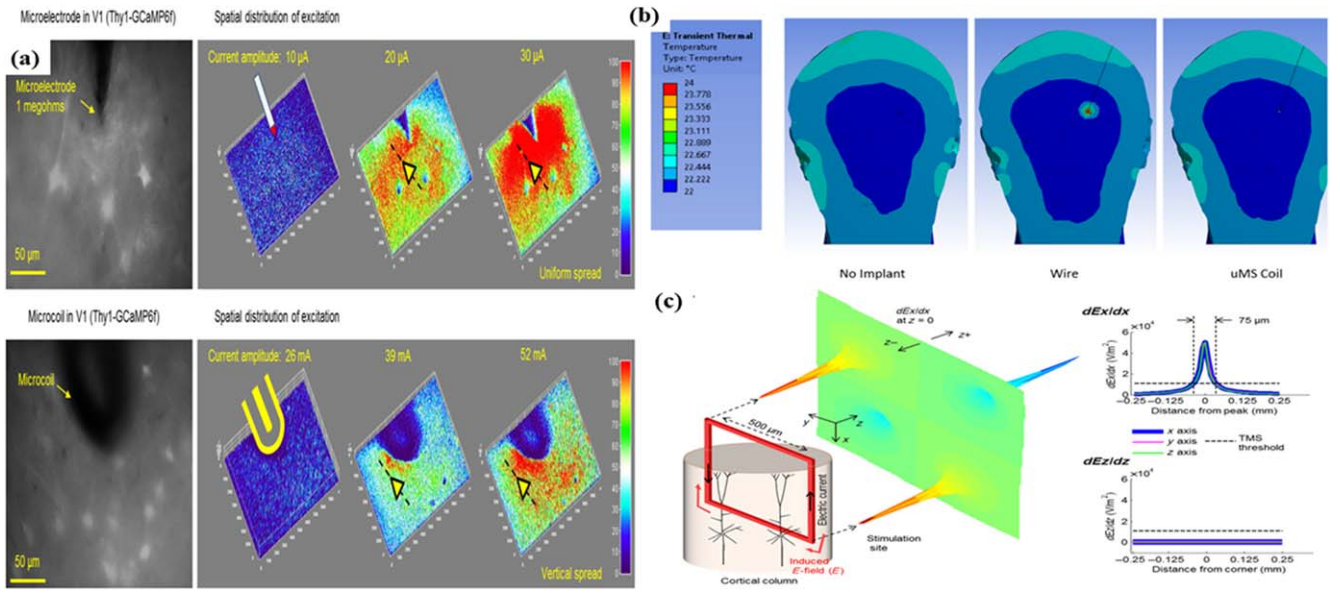

Figure 19. (a) Comparison of neural responses from electrical microelectrodes (top row) to that of magnetic μcoils (bottom row) through calcium fluorescence imaging technique. From [16]. Reprinted with permission from AAAS. (b) Simulation results for the RF induced spatial heating of the implants to compare MRI compatibility of an electrical implant and a magnetic implant. It shows, under the same circumstances, the magnetic μcoils show significantly lower heating effects on the surrounding tissues proving to be MRI compatible. Reproduced from [7]. CC BY 4.0. (c) The spatial electric field gradient of a square magnetic μcoil given by simulation results. It shows that the spatial gradient of the square μcoils is above the TMS threshold for over 75 μm from the location of the coil. From [16]. Reprinted with permission from AAAS.

mapped by calcium fluorescence imaging technique [16]. Compared to the DBS microelectrodes, that are in the size range of several mm [1] and represent a uniform spread of neuron activation, the μcoils, whose size range is in the order of several μm, not only has the advantage of smaller size of implants but also provides the benefit of selectively activating neurons. Besides, μcoil implants activate deeper neurons (60–75 μm) while the focal depth for activation in the case of microelectrodes are limited to 10 μm (see figure 19(c)). On the dark side, from figure 19(a), it is also observed that these μcoils operate on a current (52 mA) which is three orders greater than the current of operation for microelectrodes (30 μA). This signifies that μcoils may cause enhanced thermal effects on neuronal tissues, thereby hindering their application as implantable neurostimulators. The thermal effects of planar magnetic μcoils were studied through computational modeling, where Park *et al* [78] had reported the increase in temperature on gray matter of the brain remains unaffected by the number of turns of the coil, the line width and line thickness of the coil. In contrast, with the increase of the outer diameter, the thickness of the insulating layer and the interval of the pulse, the thermal effect of the gray matter is reduced [78]. Additionally, these μcoils are still too large (several hundreds of μm) to activate individual neurons. However, yet another advantage of these μcoils over microelectrodes is their MRI compatibility as reported by Bonmassar *et al* [7]. To mimic an MRI environment, the authors simulated a RF induced local heating profile for electrical implants and μcoil implants. As shown in figure 19(b), between the wire implant and the μMS implant, the former showed an increase in temperature of the surrounding tissues while the μcoil showed a heating profile more like the case where there was no implant. Finally, as discussed in section 3.3, these μcoil implants have been investigated as a potential treatment option for epilepsy across various reports [104–106].

To address the drawback in magnetic neurostimulation caused by the μcoils, spintronic nanodevices have been investigated as a promising magnetic neurostimulation implant. Although, the study of these implants has been limited to theoretical results only, they have shown extreme promise in terms of cellular-level stimulation of neurons [18, 127, 128]. The nanosecond pulsed electric fields (nsPEFs) generated from these spintronic implants have found yet another application in treatment of brain tumors as discussed in section 4.3. MNPs in neurostimulation offer non-invasive yet focused and targeted magnetic neurostimulation. The MNPs can also be controlled externally by an alternating magnetic field gradient providing an excellent precision over the region of target stimulation [21, 198].

7. Conclusive remarks

The existing techniques for the treatment of neurological disorders leave enough room for debate among drugs, non-invasive TMS, tDCS, and wearables. Undoubtedly, the use of implants is the most contentious among these, primarily because it involves an invasive, surgical procedure, as well as experienced, skilled neurosurgeons for successful implantation of these DBS leads and repeated patient monitoring after the implant surgery. In addition, DBS electrodes are MRI

Table 2. Performance statistics of the existing neurostimulators.

	Method of stimulation	Volume of the implant (in cc)	Power of implant operation (in nW)	Pros	Cons	References
Clinical DBS electrodes[a]	Electric	$\sim 10^{-3}$	$\sim 10^{8}$	Focused, localized	Implants, MRI incompatible	[1, 12]
TMS	Magnetic	$\sim 10^{4}$	$\sim 10^{16}$	Non-invasive, impressive depth of stimulation	No focal stimulation	[68, 209, 210]
Commercial μcoils	Magnetic	$\sim 10^{-1}$	$\sim 10^{9}$	Focused, high penetration depth	Implants, high power	[6, 15, 74, 104]
Fabricated μcoils	Magnetic	$\sim 10^{-6}$	$\sim 10^{6}$	Selective	Implants, no cellular resolution	[16, 17]
Nanopatterned soft magnetic material μcoils	Magnetic	$\sim 5 \times 10^{-9}$	$\sim 4.5 \times 10^{2}$	Cellular resolution	Implants, bulky	[92]
Magnetic Nanowire-based Neurostimulator (MNNS)	Magnetic	$\sim 6 \times 10^{-14}$	$\sim 2 \times 10^{8}$	Better cellular resolution	High power, high frequency	[18, 116, 129]
Spin orbit torque neurostimulator (SOTNS)	Magnetic	$\sim 8 \times 10^{-19}$	$\sim 2 \times 10^{6}$	Best cellular resolution	High frequency	[128, 144, 145, 211]
Skyrmion-based neurostimulator (SkyNS)	Magnetic	$\sim 10^{-16}$	~ 1.434	Better cellular resolution, lowest power	Difficult fabrication, high frequency	[127, 131, 139]
in vivo MNP delivery-based neurostimulation	Magnetomechanical, chemomagnetic	$\sim 3 \times 10^{6}$ particles/cc	—	Non-invasive, focal stimulation	Non-biocompatible dissociation of MNPs in the body	[20, 21]

[a] Over its several years of success in clinical settings, these electrical implants have been renamed as per its application. Special mention includes: transcutaneous electrical nerve stimulation (TENS), electrical muscle stimulation (EMS), functional electrical stimulation (FES) [212–215].

incompatible which means more dependency on expensive CT-scan, PET scan techniques for monitoring the impact of the implants on the patient's health. Yet, DBS electrodes got FDA clearance way back in 1997 and over the years, it has found its way to become a trusted treatment for Parkinson's disease, tremors and epilepsy. Implantable μMS through μcoils is a relatively new concept and the reports have been quite promising. Although the μcoils consume significantly higher current than the DBS leads and the activation of neurons at single cell level is impossible, it shows promise for selective deep activation of neurons due to high permeability of magnetic field through biological tissues. To resolve the issue of high-power consumption of the μcoils, we have reviewed the soft magnetic material-based μcoils which can significantly reduce the current consumption and meanwhile, provide a much better spatial resolution for tissue activation. Other strategies to reduce the power of operation for μMS include optimizing the stimulation pulse shape (triangular or rectangular or sinusoidal) and designing a complex circuitry to harvest the unused energy from the inductors as future wireless neurostimulators. Several research groups recently have reported studies on neurostimulation with magnetic microcoils (μcoils). The induced electric field from the time-varying magnetic field generated from these magnetic μcoils is used to remotely stimulate neighboring neurons. Due to the spatial asymmetry of the induced electric field, high spatial selectivity of neurostimulation has been realized on μcoils. However, the complications regarding high power of operation ($\sim 10^6$–109 nW) and neurostimulation at the cellular-level remain unsolved.

For the three spintronic neurostimulators (nucleation of domain walls in nanowires, field-free SOT switching and nucleation and movement of skyrmions), ultra-low power consumption and excellent cellular-level resolution of these nanodevices are their most attractive features. However, these spintronic nanodevices have a high frequency of operation (GHz range) which causes generation of nanosecond pulsed electric field (nsPEF), which is questionable for neurostimulation but opens a new research domain that promises low-power tumor therapy. It is exciting to note that magneto-ionic switching [90, 216–218, 91, 219] in the frequency range of 1 Hz promises to make spintronic neurostimulation possible.

In section 5, we reviewed an emerging neurostimulation strategy that relies on magnetic nanomaterials such as MNPs, magnetic thin films, and magnetic nanodiscs (MNDs). These magnetic nanomaterial-based neurostimulation strategies are categorized by the mechanisms such as magnetothermal, magnetomechanical, and magnetoelectrical stimulations. Compared to the counterparts of DBS electrodes, μcoils, and spintronic devices, the MNPs are intrinsically smaller and can be remotely controlled by external magnetic fields. With the recent advancements of MNP synthesis and surface biomodifications, these free-standing MNPs face less problems with the biocompatibility and neuro-interfacing issues. It can be foreseen that MNPs will be one category of invaluable neurotechnology for less invasive and more reliable neurostimulations.

Overall, this paper reviews the next generation implantable magnetic neurostimulators which can stimulate deep target neurons at the cellular level with lowered thermal effects on tissues. Although the initial success of magnetic stimulation is promising, deeper study on magnetic stimulation protocols and evaluation of long-term safety of these new implants must be made for any further advancements.

Acknowledgments

The authors would like to thank useful discussions with Dr. Sadegh Faramarzi and Prof. Theoden I. Netoff from the Department of Biomedical Engineering (UMN), Prof. Walter Low from the Department of Neurosurgery (UMN), Prof. Susan Keirstead from the Stem Cell Institute (UMN), Dr. Winfried A. Raabe, M.D. from the Department of Neurosurgery (UMN), Kendall H. Lee, M.D., PhD, Charles D. Blaha, PhD and Yoonbae Oh, PhD from Mayo Clinic, Rochester, MN.

Data availability statement

No new data were created or analysed in this study.

Notes

The authors declare no conflict of interest.

ORCID iDs

Renata Saha https://orcid.org/0000-0002-0389-0083
Kai Wu https://orcid.org/0000-0002-9444-6112
Robert P Bloom https://orcid.org/0000-0002-7781-5270
Shuang Liang https://orcid.org/0000-0003-1491-2839
Denis Tonini https://orcid.org/0000-0001-5121-5544
Jian-Ping Wang https://orcid.org/0000-0003-2815-6624

References

[1] Amon A and Alesch F 2017 Systems for deep brain stimulation: review of technical features *J. Neural Transm.* **124** 1083–91
[2] Tjong F V and Reddy V Y 2017 Permanent leadless cardiac pacemaker therapy: a comprehensive review *Circulation* **135** 1458–70
[3] Nguyen S, Cloutier F, Philippon D, Côté M, Bussieres R and Backous D D 2016 Outcomes review of modern hearing preservation technique in cochlear implant *Auris. Nasus. Larynx* **43** 485–8
[4] Hafner B J, Gaunaurd I A, Morgan S J, Amtmann D, Salem R and Gailey R S 2017 Construct validity of the Prosthetic Limb Users Survey of Mobility (PLUS-M) in adults with lower limb amputation *Arch. Phys. Med. Rehabil.* **98** 277–85

[5] Weiland J D, Cho A K and Humayun M S 2011 Retinal prostheses: current clinical results and future needs *Ophthalmology* **118** 2227–37

[6] Golestanirad L, Gale J T, Manzoor N F, Park H-J, Glait L, Haer F, Kaltenbach J A and Bonmassar G 2018 Solenoidal micromagnetic stimulation enables activation of axons with specific orientation *Front. Physiol.* **9** 724

[7] Bonmassar G and Serano P 2020 MRI-induced heating of coils for microscopic magnetic stimulation at 1.5 tesla: an initial study *Front. Hum. Neurosci.* **14** 53

[8] Iacono M I, Makris N, Mainardi L, Angelone L M and Bonmassar G 2013 MRI-based multiscale model for electromagnetic analysis in the human head with implanted DBS *Comput. Math. Methods Med.* **2013** 694171

[9] Skousen J L, Bridge M J and Tresco P A 2015 A strategy to passively reduce neuroinflammation surrounding devices implanted chronically in brain tissue by manipulating device surface permeability *Biomaterials* **36** 33–43

[10] Polikov V S, Tresco P A and Reichert W M 2005 Response of brain tissue to chronically implanted neural electrodes *J. Neurosci. Methods* **148** 1–18

[11] Wastensson G 2010 *Quantitative methods for evaluation of tremor and neuromotor function: application in workers exposed to neurotoxic metals and patients with essential tremor* Institute of Medicine. Department of Public Health and Community Medicine (https://gupea.ub.gu.se/handle/2077/23133)

[12] Waln O and Jimenez-Shahed J 2014 Rechargeable deep brain stimulation implantable pulse generators in movement disorders: patient satisfaction and conversion parameters *Neuromodulation Technol. Neural Interface* **17** 425–30

[13] Kaminska M, Perides S, Lumsden D E, Nakou V, Selway R, Ashkan K and Lin J-P 2017 Complications of deep brain stimulation (DBS) for dystonia in children–the challenges and 10 year experience in a large paediatric cohort *Eur J. Paediatr. Neurol.* **21** 168–75

[14] Walsh V and Cowey A 2000 Transcranial magnetic stimulation and cognitive neuroscience *Nat. Rev. Neurosci.* **1** 73–80

[15] Bonmassar G, Lee S W, Freeman D K, Polasek M, Fried S I and Gale J T 2012 Microscopic magnetic stimulation of neural tissue *Nat. Commun.* **3** 921

[16] Lee S W, Fallegger F, Casse B D and Fried S I 2016 Implantable microcoils for intracortical magnetic stimulation *Sci. Adv.* **2** e1600889

[17] Rizou M-E and Prodromakis T 2018 Magnetic stimulation in the microscale: The development of a 6 × 6 array of micro-coils for stimulation of excitable cells in vitro *Biomed. Phys. Eng. Express* **4** 025016

[18] Su D, Wu K, Saha R and Wang J-P 2019 Tunable magnetic domain walls for therapeutic neuromodulation at cellular level: Stimulating neurons through magnetic domain walls *J. Appl. Phys.* **126** 183902

[19] Rao S, Chen R, LaRocca A A, Christiansen M G, Senko A W, Shi C H, Chiang P-H, Varnavides G, Xue J and Zhou Y 2019 Remotely controlled chemomagnetic modulation of targeted neural circuits *Nat. Nanotechnol.* **14** 967–73

[20] Yue K, Guduru R, Hong J, Liang P, Nair M and Khizroev S 2012 Magneto-electric nano-particles for non-invasive brain stimulation *PLoS One* **7** e44040

[21] Gregurec D, Senko A W, Chuvilin A, Reddy P D, Sankararaman A, Rosenfeld D, Chiang P-H, Garcia F, Tafel I and Varnavides G 2020 Magnetic vortex nanodiscs enable remote magnetomechanical neural stimulation *ACS Nano* **14** 8036–45

[22] Lin C-W, Lin M-L, Lu S-S, Shih W-P, Wen Y-R and Chiu H-W 2011 Implantable pulsed-radiofrequency micro-stimulation system (https://patents.google.com/patent/US20110130804A1/en)

[23] Chan C and Nicholson C 1986 Modulation by applied electric fields of Purkinje and stellate cell activity in the isolated turtle cerebellum *J. Physiol.* **371** 89–114

[24] Francis J T, Gluckman B J and Schiff S J 2003 Sensitivity of neurons to weak electric fields *J. Neurosci.* **23** 7255–61

[25] Cejnar P, Vyšata O, Kukal J, Beránek M, Vališ M and Procházka A 2020 Simple capacitor-switch model of excitatory and inhibitory neuron with all parts biologically explained allows input fire pattern dependent chaotic oscillations *Sci. Rep.* **10** 1–18

[26] Pereda A E 2014 Electrical synapses and their functional interactions with chemical synapses *Nat. Rev. Neurosci.* **15** 250–63

[27] Feiner A-S and McEvoy A 1994 The nernst equation *J. Chem. Educ.* **71** 493

[28] Roland C G 1973 Nobel lectures, including presentation speeches and laureates Biographies: Physiology or Medicine 1963-1970 *JAMA* **226** 1124

[29] Wang Y and Guo L 2016 Nanomaterial-enabled neural stimulation *Front. Neurosci.* **10** 69

[30] Fletcher A 2011 Action potential: generation and propagation *Anaesth. Intensive Care Med.* **12** 258–62

[31] Hoogerwerf A C and Wise K D 1994 A three-dimensional microelectrode array for chronic neural recording *IEEE Trans. Biomed. Eng.* **41** 1136–46

[32] Maynard E M, Nordhausen C T and Normann R A 1997 The Utah intracortical electrode array: a recording structure for potential brain-computer interfaces *Electroencephalogr. Clin. Neurophysiol.* **102** 228–39

[33] Hideharu H and Haruo M 1994 Fluorescence imaging of intracellular Ca^{2+} *J. Pharmacol. Toxicol. Methods* **31** 1–10

[34] Tian L, Hires S A, Mao T, Huber D, Chiappe M E, Chalasani S H, Petreanu L, Akerboom J, McKinney S A and Schreiter E R 2009 Imaging neural activity in worms, flies and mice with improved GCaMP calcium indicators *Nat. Methods* **6** 875–81

[35] Valley M T, Moore M G, Zhuang J, Mesa N, Castelli D, Sullivan D, Reimers M and Waters J 2020 Separation of hemodynamic signals from GCaMP fluorescence measured with wide-field imaging *J. Neurophysiol.* **123** 356–66

[36] Shuttleworth C W 2010 Use of NAD (P) H and flavoprotein autofluorescence transients to probe neuron and astrocyte responses to synaptic activation *Neurochem. Int.* **56** 379–86

[37] Reinert K C, Gao W, Chen G and Ebner T J 2007 Flavoprotein autofluorescence imaging in the cerebellar cortex *in vivo J. Neurosci. Res.* **85** 3221–32

[38] Carter M E and de Lecea L 2011 Optogenetic investigation of neural circuits *in vivo Trends Mol. Med.* **17** 197–206

[39] Mancuso J J, Kim J, Lee S, Tsuda S, Chow N B and Augustine G J 2011 Optogenetic probing of functional brain circuitry *Exp. Physiol.* **96** 26–33

[40] Asrican B, Augustine G J, Berglund K, Chen S, Chow N, Deisseroth K, Feng G, Gloss B, Hira R and Hoffmann C 2013 Next-generation transgenic mice for optogenetic analysis of neural circuits *Front. Neural Circuits* **7** 160

[41] Bah E, Hachmann J, Paek S B, Batton A, Min P K, Bennet K and Lee K 2017 Wireless intraoperative real-time monitoring of neurotransmitters in humans 2017 *IEEE Int. Symp. on Medical Measurements and Applications (MeMeA) (IEEE) pp 123–8*

[42] Kokkinos V, Sisterson N D, Wozny T A and Richardson R M 2019 Association of closed-loop brain stimulation neurophysiological features with seizure control among patients with focal epilepsy *JAMA Neurol.* **76** 800–8

[43] Cheung T P, Grunau R E, Synnes A, Eswaran H and Doesburg S M 2015 Magnetoencephalography:

neurophysiologic imaging for perinatal brain development *NeoReviews* **16** e544–50
[44] Booker S A, Song J and Vida I 2014 Whole-cell patch-clamp recordings from morphologically-and neurochemically-identified hippocampal interneurons *J. Vis. Exp.* **91** e51706
[45] Kipke D R, Shain W, Buzsáki G, Fetz E, Henderson J M, Hetke J F and Schalk G 2008 Advanced neurotechnologies for chronic neural interfaces: new horizons and clinical opportunities *J. Neurosci.* **28** 11830–8
[46] Hinrichs H, Scholz M, Baum A K, Kam J W, Knight R T and Heinze H-J 2020 Comparison between a wireless dry electrode EEG system with a conventional wired wet electrode EEG system for clinical applications *Sci. Rep.* **10** 1–14
[47] Roberts T P, Paulson D N, Hirschkoff G, Pratt K, Mascarenas A, Miller P, Han M, Caffrey J, Kincade C and Power W 2014 Artemis 123: development of a whole-head infant and young child MEG system *Front. Hum. Neurosci.* **8** 99
[48] Matsui Y, Sakurai J, Hiraki T, Okamoto S, Iguchi T, Tomita K, Uka M, Gobara H and Kanazawa S 2019 MRI-guided percutaneous needle biopsy with 1.2 T open MRI: study protocol for a prospective feasibility study (SCIRO-1701) *Nagoya J. Med. Sci.* **81** 463
[49] McGlynn E, Nabaei V, Ren E, Galeote-Checa G, Das R, Curia G and Heidari H 2021 The future of neuroscience: flexible and wireless implantable neural electronics *Adv. Sci.* **8** 2002693
[50] Gilgunn P, Khilwani R, Kozai T, Weber D, Cui X, Erdos G, Ozdoganlar O and Fedder G 2012 An ultra-compliant, scalable neural probe with molded biodissolvable delivery vehicle 2012 *IEEE 25th Int. Conf. on Micro Electro Mechanical Systems (MEMS) (IEEE)* pp 56–9
[51] Vachicouras N, Tarabichi O, Kanumuri V V, Tringides C M, Macron J, Fallegger F, Thenaisie Y, Epprecht L, McInturff S and Qureshi A A 2019 Microstructured thin-film electrode technology enables proof of concept of scalable, soft auditory brainstem implants *Sci. Transl. Med.* **11** eaax9487
[52] Luan L, Robinson J T, Aazhang B, Chi T, Yang K, Li X, Rathore H, Singer A, Yellapantula S and Fan Y 2020 Recent advances in electrical neural Interface engineering: Minimal invasiveness, longevity, and scalability *Neuron* **108** 302–21
[53] Guo L, Guvanasen G S, Liu X, Tuthill C, Nichols T R and DeWeerth S P 2012 A PDMS-based integrated stretchable microelectrode array (isMEA) for neural and muscular surface interfacing *IEEE Trans. Biomed. Circuits Syst.* **7** 1–10
[54] Adly N, Weidlich S, Seyock S, Brings F, Yakushenko A, Offenhäusser A and Wolfrum B 2018 Printed microelectrode arrays on soft materials: from PDMS to hydrogels *Npj Flex. Electron.* **2** 1–9
[55] Lee K, He J, Clement R, Massia S and Kim B 2004 Biocompatible benzocyclobutene (BCB)-based neural implants with micro-fluidic channel *Biosens. Bioelectron.* **20** 404–7
[56] Zhu H, He J and Kim B 2004 High-yield Benzocyclobutene (BCB) based neural implants for simultaneous intra-And extracortical recording in rats *The 26th Annual Int. Conf. of the IEEE Engineering in Medicine and Biology Society vol 2 (IEEE)* 4341–4
[57] Li W, Rodger D C, Pinto A, Meng E, Weiland J D, Humayun M S and Tai Y-C 2011 Parylene-based integrated wireless single-channel neurostimulator *Sens. Actuators Phys.* **166** 193–200
[58] Xie X, Rieth L, Williams L, Negi S, Bhandari R, Caldwell R, Sharma R, Tathireddy P and Solzbacher F 2014 Long-term reliability of Al_2O_3 and Parylene C bilayer encapsulated Utah electrode array based neural interfaces for chronic implantation *J. Neural Eng.* **11** 026016
[59] Caldwell R, Street M G, Sharma R, Takmakov P, Baker B and Rieth L 2020 Characterization of Parylene-C degradation mechanisms: In vitro reactive accelerated aging model compared to multiyear *in vivo* implantation *Biomaterials* **232** 119731
[60] Lee K, Singh A, He J, Massia S, Kim B and Raupp G 2004 Polyimide based neural implants with stiffness improvement *Sensors Actuators B* **102** 67–72
[61] Rubehn B and Stieglitz T 2010 In vitro evaluation of the long-term stability of polyimide as a material for neural implants *Biomaterials* **31** 3449–58
[62] Vomero M, Cruz M F P, Zucchini E, Shabanian A, Delfino E, Carli S, Fadiga L, Ricci D and Stieglitz T 2018 Achieving ultra-conformability with polyimide-based ECoG arrays 2018 *40th Annual Int. Conf. of the IEEE Engineering in Medicine and Biology Society (EMBC) (IEEE)* pp 4464–7
[63] Shi J and Fang Y 2019 Flexible and implantable microelectrodes for chronically stable neural interfaces *Adv. Mater.* **31** 1804895
[64] Seaton B T, Hill D F, Cowen S L and Heien M L 2020 Mitigating the effects of electrode biofouling-induced impedance for improved long-term electrochemical measurements in vivo *Anal. Chem.* **92** 6334–40
[65] Vingerhoets F J, Villemure J-G, Temperli P, Pollo C, Pralong E and Ghika J 2002 Subthalamic DBS replaces levodopa in Parkinson's disease: two-year follow-up *Neurology* **58** 396–401
[66] Justesen D R and Guy A 1985 Arsene Jacques d'Arsonval: a brief history *Bioelectromagn J. Bioelectromagn. Soc. Soc. Phys. Regul. Biol. Med. Eur. Bioelectromagn. Assoc.* **6** 111–4
[67] Campbell Swinton A A 1920 A Silvanus Phillips Thompson, D.Sc., LL.D., F.R.S. His Life and Letters *Nature* **105** 448–9
[68] Guadagnin V, Parazzini M, Fiocchi S, Liorni I and Ravazzani P 2015 Deep transcranial magnetic stimulation: modeling of different coil configurations *IEEE Trans. Biomed. Eng.* **63** 1543–50
[69] Tenforde T 1991 Biological interactions of extremely-low-frequency electric and magnetic fields *J. Electroanal. Chem. Interfacial Electrochem.* **320** 1–17
[70] Fitch M T and Silver J 2008 CNS injury, glial scars, and inflammation: Inhibitory extracellular matrices and regeneration failure *Exp. Neurol.* **209** 294–301
[71] Salatino J W, Ludwig K A, Kozai T D and Purcell E K 2017 Glial responses to implanted electrodes in the brain *Nat. Biomed. Eng.* **1** 862–77
[72] Lee S W, Thyagarajan K and Fried S I 2018 Micro-Coil design influences the spatial extent of responses to intracortical magnetic stimulation *IEEE Trans. Biomed. Eng.* **66** 1680–94
[73] Jeong H, Deng J and Bonmassar G 2021 Planar figure-8 coils for ultra-focal and directional micromagnetic brain stimulation *J. Vac. Sci. Technol. B* **39** 063202
[74] Park H-J, Bonmassar G, Kaltenbach J A, Machado A G, Manzoor N F and Gale J T 2013 Activation of the central nervous system induced by micro-magnetic stimulation *Nat. Commun.* **4** 2463
[75] Khalifa A, Zaeimbashi M, Zhou T X, Abrishami S M, Sun N, Park S, Šumarac T, Qu J, Zohar I and Yacoby A 2021 The development of microfabricated solenoids with magnetic cores for micromagnetic neural stimulation *Microsyst. Nanoeng.* **7** 1–10
[76] Lee S W and Fried S I 2014 The response of L5 pyramidal neurons of the PFC to magnetic stimulation from a micro-coil 2014 *36th Annual Int. Conf. of the IEEE Engineering in Medicine and Biology Society (IEEE)* pp 6125–8

[77] Saha R *et al* 2021 Strength-frequency curve for micromagnetic neurostimulation through EPSPs on rat hippocampal neurons and numerical modeling of magnetic microcoil (μcoil) *Journal of Neural Engineering* (https://doi.org/10.1088/1741-2552/ac4baf/meta)

[78] Park H-J, Seol J H, Ku J and Kim S 2015 Computational study on the thermal effects of implantable magnetic stimulation based on planar coils *IEEE Trans. Biomed. Eng.* **63** 158–67

[79] Osanai H, Minusa S and Tateno T 2018 Micro-coil-induced inhomogeneous electric field produces sound-driven-like neural responses in microcircuits of the mouse auditory cortex in v*ivo Neuroscience* **371** 346–70

[80] Mukesh S, Zeller-Townson R, Butera R J and Bhatti P T 2019 *Magnetic stimulation of dissociated cortical neurons on a planar mulitelectrode array 2019 9th Int. IEEE/EMBS Conf. on Neural Engineering (NER) (IEEE)* pp 758–61

[81] Minusa S, Muramatsu S, Osanai H and Tateno T 2019 A multichannel magnetic stimulation system using submillimeter-sized coils: system development and experimental application to rodent brain *in vivo J. Neural Eng.* **16** 066014

[82] Lee S W and Fried S I 2016 Enhanced control of cortical pyramidal neurons with micromagnetic stimulation *IEEE Trans. Neural Syst. Rehabil. Eng.* **25** 1375–86

[83] Minusa S, Osanai H and Tateno T 2017 Micromagnetic stimulation of the mouse auditory cortex *in vivo* using an implantable solenoid system *IEEE Trans. Biomed. Eng.* **65** 1301–10

[84] Dong L, Li G, Tian C, Lin L, Gao Y and Zheng Y 2021 Design of Submillimeter Magnetic Stimulation Instrumentation and Its Targeted Inhibitory Effect on Rat Model of Epilepsy *IEEE Trans. Instrum. Meas.* **70** 1–8

[85] Ye H, Chen V C-F, Helon J and Apostolopoulos N 2020 Focal suppression of epileptiform activity in the hippocampus by a high-frequency magnetic field *Neuroscience* **432** 1–14

[86] Lee S W and Fried S I 2015 Magnetic control of cortical pyramidal neuron activity using a micro-coil 2015 *7th Int. IEEE/EMBS Conf. on Neural Engineering (NER) (IEEE)* pp 268–71

[87] Tian L, Song L, Zheng Y, Wang J and Chen H 2020 An improved F/C structure for cell-scale micro-magnetic coil *IEEE Trans. Magn.* **56** 1–8

[88] Hochstein P, Kumar K S and Forman S J 1980 Lipid peroxidation and the cytotoxicity of copper *Ann. New York Acad. Sci.* **355** 240–8

[89] Armstrong C, Leong W and Lees G J 2001 Comparative effects of metal chelating agents on the neuronal cytotoxicity induced by copper (Cu + 2), iron (Fe + 3) and zinc in the hippocampus *Brain Res.* **892** 51–62

[90] Sahu P, Zhang D, Peterson T and Wang J-P 2020 Effects of mobile oxygen ions in top-gated synthetic antiferromagnet structure *Appl. Phys. Lett.* **117** 202405

[91] Saha R, Shiao M-L, Bloom R-P, Benally O-J, Faramarji S, Wu K, Girolamo A, Tonini D, Netoff T-I, Low W, Keistead S, Wang J-P *et al* Planar microcoils as cellular-level micromagnetic neurostimulators in preparation

[92] Ramadan Q, Samper V D, Puiu D P and Yu C 2006 Fabrication of three-dimensional magnetic microdevices with embedded microcoils for magnetic potential concentration *J. Microelectromech. Syst.* **15** 624–38

[93] Niarchos D 2003 Magnetic MEMS: key issues and some applications *Sens. Actuators Phys.* **109** 166–73

[94] Dong T, Su Q, Yang Z, Zhang Y, Egeland E B, Gu D D, Calabrese P, Kapiris M J, Karlsen F and Minh N T 2010 A smart fully integrated micromachined separator with soft magnetic micro-pillar arrays for cell isolation *J. Micromech. Microeng.* **20** 115021

[95] Donahue M 1999 *OOMMF User's Guide, Version 1.0* 6376 (Gaithersburg, MD: National Institute of Standards and Technology) (https://doi.org/10.6028/NIST.IR.6376)

[96] Vansteenkiste A, Leliaert J, Dvornik M, Helsen M, Garcia-Sanchez F and Van Waeyenberge B 2014 The design and verification of MuMax3 *AIP Adv.* **4** 107133

[97] Wang J-P, Saha R, Su D and Wu K Nanopatterned soft magnetic material-based microcoil for highly focused, low-power, implantable magnetic stimulation PCT Application No. PCT/US2021/025322

[98] Le H T, Haque R I, Ouyang Z, Lee S W, Fried S I, Zhao D, Qiu M and Han A 2021 MEMS inductor fabrication and emerging applications in power electronics and neurotechnologies *Microsyst. Nanoeng.* **7** 1–22

[99] Sarreal R R and Bhatti P 2020 Characterization and miniaturization of silver-nanoparticle microcoil via aerosol jet printing techniques for micromagnetic cochlear stimulation *Sensors* **20** 6087

[100] Zhang T, Wang X, Li T, Guo Q and Yang J 2014 Fabrication of flexible copper-based electronics with high-resolution and high-conductivity on paper via inkjet printing *J. Mater. Chem. C* **2** 286–94

[101] Ha C W, Prabhakaran P and Son Y 2019 3D-printed polymer/metal hybrid microstructures with ultraprecision for 3D microcoils *3D Print. Addit. Manuf.* **6** 165–70

[102] Meier R C, Höfflin J, Badilita V, Wallrabe U and Korvink J G 2014 Microfluidic integration of wirebonded microcoils for on-chip applications in nuclear magnetic resonance *J. Micromech. Microeng.* **24** 045021

[103] Wang N, Meissner M, MacKinnon N, Luchnikov V, Mager D and Korvink J 2017 Fast prototyping of microtubes with embedded sensing elements made possible with an inkjet printing and rolling process *J. Micromech. Microeng.* **28** 025003

[104] Lee S W and Fried S I 2014 Suppression of subthalamic nucleus activity by micromagnetic stimulation *IEEE Trans. Neural Syst. Rehabil. Eng.* **23** 116–27

[105] Skach J, Conway C, Barrett L and Ye H 2020 Axonal blockage with microscopic magnetic stimulation *Sci. Rep.* **10** 1–18

[106] Ye H and Barrett L 2021 Somatic inhibition by microscopic magnetic stimulation *Sci. Rep.* **11** 1–18

[107] Johnson M and Silsbee R H 1985 Interfacial charge-spin coupling: Injection and detection of spin magnetization in metals *Phys. Rev. Lett.* **55** 1790

[108] Baibich M N, Broto J M, Fert A, Van Dau F N, Petroff F, Etienne P, Creuzet G, Friederich A and Chazelas J 1988 Giant magnetoresistance of (001) Fe/(001) Cr magnetic superlattices *Phys. Rev. Lett.* **61** 2472

[109] Puebla J, Kim J, Kondou K and Otani Y 2020 Spintronic devices for energy-efficient data storage and energy harvesting *Commun. Mater.* **1** 1–9 (https://www.nature.com/articles/s43246-020-0022-5)

[110] Ranjan A, Venkataramani S, Fong X, Roy K and Raghunathan A 2015 Approximate storage for energy efficient spintronic memories 2015 *52nd ACM/EDAC/IEEE Design Automation Conf. (DAC) (IEEE)* pp 1–6

[111] Burkard G, Engel H and Loss D 2000 Spintronics and quantum dots for quantum computing and quantum communication *Fortschritte Phys. Prog. Phys.* **48** 965–86

[112] Cerletti V, Coish W, Gywat O and Loss D 2005 Recipes for spin-based quantum computing *Nanotechnology* **16** R27

[113] Torrejon J, Riou M, Araujo F A, Tsunegi S, Khalsa G, Querlioz D, Bortolotti P, Cros V, Yakushiji K and Fukushima A 2017 Neuromorphic computing with nanoscale spintronic oscillators *Nature* **547** 428–31

[114] Grollier J, Querlioz D, Camsari K, Everschor-Sitte K, Fukami S and Stiles M D 2020 Neuromorphic spintronics *Nat. Electron.* **3** 360–70

[115] Kurenkov A, Fukami S and Ohno H 2020 Neuromorphic computing with antiferromagnetic spintronics *J. Appl. Phys.* **128** 010902
[116] Wang J, Low W C and Mahendra D 2016 Magnetic nanostimulator and nanosensor array for biological material stimulation and sensing (https://patents.google.com/patent/US10201715B2/en)
[117] Kang W, Zhang Y, Wang Z, Klein J-O, Chappert C, Ravelosona D, Wang G, Zhang Y and Zhao W 2015 Spintronics: Emerging ultra-low-power circuits and systems beyond MOS technology *ACM J. Emerg. Technol. Comput. Syst. JETC* **12** 16
[118] Zhang Y, Zhao W, Klein J-O, Kang W, Querlioz D, Zhang Y, Ravelosona D and Chappert C 2014 *Spintronics for low-power computing Proc. of the Conf. on Design, Automation & Test in Europe (European Design and Automation Association)* p 303
[119] Hao Z, Yuan-Yuan L, Mei-Yin Y, Bao Z, Guang Y, Shou-Guo W and Kai-You W 2015 Tuning the magnetic anisotropy of CoFeB grown on flexible substrates *Chin. Phys. B* **24** 077501
[120] Vemulkar T, Mansell R, Fernández-Pacheco A and Cowburn R 2016 Toward flexible spintronics: perpendicularly magnetized synthetic antiferromagnetic thin films and nanowires on polyimide substrates *Adv. Funct. Mater.* **26** 4704–11
[121] Beach G S, Nistor C, Knutson C, Tsoi M and Erskine J L 2005 Dynamics of field-driven domain-wall propagation in ferromagnetic nanowires *Nat. Mater.* **4** 741
[122] Miron I M, Moore T, Szambolics H, Buda-Prejbeanu L D, Auffret S, Rodmacq B, Pizzini S, Vogel J, Bonfim M and Schuhl A 2011 Fast current-induced domain-wall motion controlled by the rashba effect *Nat. Mater.* **10** 419
[123] Ai J, Miao B, Sun L, You B, Hu A and Ding H 2011 Current-induced domain wall motion in permalloy nanowires with a rectangular cross-section *J. Appl. Phys.* **110** 093913
[124] Jamali M, Yang H and Lee K-J 2010 Spin wave assisted current induced magnetic domain wall motion *Appl. Phys. Lett.* **96** 242501
[125] Koyama T, Chiba D, Ueda K, Tanigawa H, Fukami S, Suzuki T, Ohshima N, Ishiwata N, Nakatani Y and Ono T 2011 Magnetic field insensitivity of magnetic domain wall velocity induced by electrical current in Co/Ni nanowire *Appl. Phys. Lett.* **98** 192509
[126] Koyama T, Chiba D, Ueda K, Kondou K, Tanigawa H, Fukami S, Suzuki T, Ohshima N, Ishiwata N and Nakatani Y 2011 Observation of the intrinsic pinning of a magnetic domain wall in a ferromagnetic nanowire *Nat. Mater.* **10** 194
[127] Saha R, Wu K, Su D and Wang J-P 2019 Tunable magnetic skyrmions in spintronic nanostructures for cellular-level magnetic neurostimulation *J. Phys. Appl. Phys.* **52** 465002
[128] Wu K, Su D, Saha R and Wang J-P 2019 Spin–orbit torque and spin hall effect-based cellular level therapeutic spintronic neuromodulator: a simulation study *J. Phys. Chem. C* **123** 24963–72
[129] Yamaguchi A, Ono T, Nasu S, Miyake K, Mibu K and Shinjo T 2004 Real-space observation of current-driven domain wall motion in submicron magnetic wires *Phys. Rev. Lett.* **92** 077205
[130] Mühlbauer S, Binz B, Jonietz F, Pfleiderer C, Rosch A, Neubauer A, Georgii R and Böni P 2009 Skyrmion lattice in a chiral magnet *Science* **323** 915–9
[131] Huang Y, Kang W, Zhang X, Zhou Y and Zhao W 2017 Magnetic skyrmion-based synaptic devices *Nanotechnology* **28** 08LT02
[132] Jiang W, Chen G, Liu K, Zang J, Te Velthuis S G and Hoffmann A 2017 Skyrmions in magnetic multilayers *Phys. Rep.* **704** 1–49
[133] He Z and Fan D 2017 A tunable magnetic skyrmion neuron cluster for energy efficient artificial neural network design *Automation & Test in Europe Conf. & Exhibition (DATE), 2017 (IEEE)* pp 350–5
[134] Fert A, Reyren N and Cros V 2017 Magnetic skyrmions: advances in physics and potential applications *Nat. Rev. Mater.* **2** 17031
[135] Jiang W, Upadhyaya P, Zhang W, Yu G, Jungfleisch M B, Fradin F Y, Pearson J E, Tserkovnyak Y, Wang K L and Heinonen O 2015 Blowing magnetic skyrmion bubbles *Science* **349** 283–6
[136] Zhang X, Zhou Y, Ezawa M, Zhao G and Zhao W 2015 Magnetic skyrmion transistor: skyrmion motion in a voltage-gated nanotrack *Sci. Rep.* **5** 11369
[137] Sampaio J, Cros V, Rohart S, Thiaville A and Fert A 2013 Nucleation, stability and current-induced motion of isolated magnetic skyrmions in nanostructures *Nat. Nanotechnol.* **8** 839
[138] Zhang X, Zhou Y and Ezawa M 2016 Antiferromagnetic skyrmion: stability, creation and manipulation *Sci. Rep.* **6** 24795
[139] Büttner F, Lemesh I, Schneider M, Pfau B, Günther C M, Hessing P, Geilhufe J, Caretta L, Engel D and Krüger B 2017 Field-free deterministic ultrafast creation of magnetic skyrmions by spin–orbit torques *Nat. Nanotechnol.* **12** 1040
[140] Liu L, Pai C-F, Li Y, Tseng H, Ralph D and Buhrman R 2012 Spin-torque switching with the giant spin Hall effect of tantalum *Science* **336** 555–8
[141] Kim J, Sheng P, Takahashi S, Mitani S and Hayashi M 2016 Spin Hall magnetoresistance in metallic bilayers *Phys. Rev. Lett.* **116** 097201
[142] Zhang S S-L and Vignale G 2016 Theory of unidirectional spin Hall magnetoresistance in heavy-metal/ferromagnetic-metal bilayers *Phys. Rev. B* **94** 140411
[143] Avci C O, Garello K, Mendil J, Ghosh A, Blasakis N, Gabureac M, Trassin M, Fiebig M and Gambardella P 2015 Magnetoresistance of heavy and light metal/ferromagnet bilayers *Appl. Phys. Lett.* **107** 192405
[144] Fukami S, Zhang C, DuttaGupta S, Kurenkov A and Ohno H 2016 Magnetization switching by spin–orbit torque in an antiferromagnet–ferromagnet bilayer system *Nat. Mater.* **15** 535
[145] Oh Y-W, Baek S C, Kim Y, Lee H Y, Lee K-D, Yang C-G, Park E-S, Lee K-S, Kim K-W and Go G 2016 Field-free switching of perpendicular magnetization through spin–orbit torque in antiferromagnet/ferromagnet/oxide structures *Nat. Nanotechnol.* **11** 878
[146] Zhang W, Jungfleisch M B, Jiang W, Pearson J E, Hoffmann A, Freimuth F and Mokrousov Y 2014 Spin Hall effects in metallic antiferromagnets *Phys. Rev. Lett.* **113** 196602
[147] Şahin C and Flatté M E 2015 Tunable giant spin Hall conductivities in a strong spin-orbit semimetal: $Bi_{1-x}Sb_x$ *Phys. Rev. Lett.* **114** 107201
[148] Sun Y, Zhang Y, Felser C and Yan B 2016 Strong intrinsic spin Hall effect in the TaAs family of Weyl semimetals *Phys. Rev. Lett.* **117** 146403
[149] Miron I M, Garello K, Gaudin G, Zermatten P-J, Costache M V, Auffret S, Bandiera S, Rodmacq B, Schuhl A and Gambardella P 2011 Perpendicular switching of a single ferromagnetic layer induced by in-plane current injection *Nature* **476** 189
[150] Lau Y-C, Betto D, Rode K, Coey J and Stamenov P 2016 Spin–orbit torque switching without an external field using interlayer exchange coupling *Nat. Nanotechnol.* **11** 758
[151] You L, Lee O, Bhowmik D, Labanowski D, Hong J, Bokor J and Salahuddin S 2015 Switching of perpendicularly polarized nanomagnets with spin orbit

torque without an external magnetic field by engineering a tilted anisotropy *Proc. Natl Acad. Sci.* **112** 10310–5
[152] Wang M, Cai W, Zhu D, Wang Z, Kan J, Zhao Z, Cao K, Wang Z, Zhang Y and Zhang T 2018 Field-free switching of a perpendicular magnetic tunnel junction through the interplay of spin–orbit and spin-transfer torques *Nat. Electron.* **1** 582
[153] Keffer F, Kaplan H and Yafet Y 1953 Spin waves in ferromagnetic and antiferromagnetic materials *Am. J. Phys.* **21** 250–7
[154] Lee K-S, Lee S-W, Min B-C and Lee K-J 2013 Threshold current for switching of a perpendicular magnetic layer induced by spin Hall effect *Appl. Phys. Lett.* **102** 112410
[155] Lian J, Bikson M, Sciortino C, Stacey W C and Durand D M 2003 Local suppression of epileptiform activity by electrical stimulation in rat hippocampus in vitro *J. Physiol.* **547** 427–34
[156] Bikson M, Lian J, Hahn P J, Stacey W C, Sciortino C and Durand D M 2001 Suppression of epileptiform activity by high frequency sinusoidal fields in rat hippocampal slices *J. Physiol.* **531** 181–91
[157] Cullen C L and Young K M 2016 How does transcranial magnetic stimulation influence glial cells in the central nervous system ? *Front. Neural Circuits* **10** 26
[158] Fang Z-Y, Li Z, Xiong L, Huang J and Huang X-L 2010 Magnetic stimulation influences injury-induced migration of white matter astrocytes *Electromagn. Biol. Med.* **29** 113–21
[159] Rauš S, Selaković V, Manojlović-Stojanoski M, Radenović L, Prolić Z and Janać B 2013 Response of hippocampal neurons and glial cells to alternating magnetic field in gerbils Unpublished to global cerebral ischemia *Neurotox. Res.* **23** 79–91
[160] Kim J Y, Choi G-S, Cho Y-W, Cho H, Hwang S-J and Ahn S-H 2013 Attenuation of spinal cord injury-induced astroglial and microglial activation by repetitive transcranial magnetic stimulation in rats *J. Korean Med. Sci.* **28** 295–9
[161] Liebetanz D, Fauser S, Michaelis T, Czeh B, Watanabe T, Paulus W, Frahm J and Fuchs E 2003 Safety aspects of chronic low-frequency transcranial magnetic stimulation based on localized proton magnetic resonance spectroscopy and histology of the rat brain *J. Psychiatr. Res.* **37** 277–86
[162] Roth C C, Payne J A, Kuipers M A, Thompson G L, Wilmink G J and Ibey B L 2012 Impact of nanosecond pulsed electric fields on primary hippocampal neurons photonic therapeutics and diagnostics VIII *Int. Soc. Opt. Photonics* **8207** 820763
[163] Gianulis E C, Casciola M, Zhou C, Yang E, Xiao S and Pakhomov A G 2019 Selective distant electrostimulation by synchronized bipolar nanosecond pulses *Sci. Rep.* **9** 1–10
[164] Delso C, Martínez J M, Cebrián G, Álvarez I and Raso J 2020 Understanding the occurrence of tailing in survival curves of Salmonella Typhimurium treated by pulsed electric fields *Bioelectrochemistry* **135** 107580
[165] Nuccitelli R, Pliquett U, Chen X, Ford W, Swanson R J, Beebe S J, Kolb J F and Schoenbach K H 2006 Nanosecond pulsed electric fields cause melanomas to self-destruct *Biochem. Biophys. Res. Commun.* **343** 351–60
[166] Pakhomov A G, Semenov I, Casciola M and Xiao S 2017 Neuronal excitation and permeabilization by 200-ns pulsed electric field: An optical membrane potential study with FluoVolt dye *Biochim. Biophys. Acta BBA-Biomembr.* **1859** 1273–81
[167] Casciola M, Xiao S and Pakhomov A G 2017 Damage-free peripheral nerve stimulation by 12-ns pulsed electric field *Sci. Rep.* **7** 10453
[168] Romanenko S, Arnaud-Cormos D, Leveque P and O'Connor R P 2016 Ultrashort pulsed electric fields induce action potentials in neurons when applied at axon bundles *2016 9th Int. Kharkiv Symp. on Physics and Engineering of Microwaves, Millimeter and Submillimeter Waves (MSMW) (IEEE)* pp 1–5
[169] Lin C-Y, Lou W-S, Chen J-C, Weng K-Y, Shih M-C, Hung Y-W, Chen Z-Y and Wang M-C 2020 Bio-compatibility and bio-insulation of implantable electrode prosthesis ameliorated by A-174 silane primed parylene-C deposited embedment *Micromachines* **11** 1064
[170] Krüger B and Kläui M 2016 Topological defects in nanostructures—chiral domain walls and skyrmions *Topological Structures in Ferroic Materials* (Berlin: Springer) pp 199–218
[171] Oldroyd P and Malliaras G 2021 Achieving long-term stability of thin-film electrodes for neurostimulation *Acta Biomater.* (In Press) (https://doi.org/10.1016/j.actbio.2021.05.004)
[172] Xu Z, Xu J, Yang W, Lin H and Ruan G 2020 Remote neurostimulation with physical fields at cellular level enabled by nanomaterials: toward medical applications *APL Bioeng.* **4** 040901
[173] Colombo E, Feyen P, Antognazza M R, Lanzani G and Benfenati F 2016 Nanoparticles: a challenging vehicle for neural stimulation *Front. Neurosci.* **10** 105
[174] Huang H, Delikanli S, Zeng H, Ferkey D M and Pralle A 2010 Remote control of ion channels and neurons through magnetic-field heating of nanoparticles *Nat. Nanotechnol.* **5** 602–6
[175] Wu K, Su D, Liu J, Saha R and Wang J-P 2019 Magnetic nanoparticles in nanomedicine: a review of recent advances *Nanotechnology* **30** 502003
[176] Serrano García R, Stafford S and Gun'ko Y K 2018 Recent progress in synthesis and functionalization of multimodal fluorescent-magnetic nanoparticles for biological applications *Appl. Sci.* **8** 172
[177] Ansari S A M K, Ficiarà E, Ruffinatti F A, Stura I, Argenziano M, Abollino O, Cavalli R, Guiot C and D'Agata F 2019 Magnetic iron oxide nanoparticles: synthesis, characterization and functionalization for biomedical applications in the central nervous system *Materials* **12** 465
[178] Shapiro M G, Homma K, Villarreal S, Richter C-P and Bezanilla F 2012 Infrared light excites cells by changing their electrical capacitance *Nat. Commun.* **3** 1–11
[179] Puglisi J L, Yuan W, Bassani J W and Bers D M 1999 Ca^{2+} influx through Ca^{2+} channels in rabbit ventricular myocytes during action potential clamp: influence of temperature *Circ. Res.* **85** e7–16
[180] Eom K, Kim J, Choi J M, Kang T, Chang J W, Byun K M, Jun S B and Kim S J 2014 Enhanced infrared neural stimulation using localized surface plasmon resonance of gold nanorods *Small* **10** 3853–7
[181] Ermakova Y G, Lanin A A, Fedotov I V, Roshchin M, Kelmanson I V, Kulik D, Bogdanova Y A, Shokhina A G, Bilan D S and Staroverov D B 2017 Thermogenetic neurostimulation with single-cell resolution *Nat. Commun.* **8** 1–15
[182] Xia Q and Nyberg T 2019 Inhibition of cortical neural networks using infrared laser *J. Biophotonics* **12** e201800403
[183] Duke A R, Jenkins M W, Lu H, McManus J M, Chiel H J and Jansen E D 2013 Transient and selective suppression of neural activity with infrared light *Sci. Rep.* **3** 1–8
[184] Fekete Z, Horváth Á C and Zátonyi A 2020 Infrared neuromodulation: a neuroengineering perspective *J. Neural Eng.* **17** 051003
[185] Jiang Y, Parameswaran R, Li X, Carvalho-de-Souza J L, Gao X, Meng L, Bezanilla F, Shepherd G M and Tian B 2019 Nongenetic optical neuromodulation with silicon-based materials *Nat. Protoc.* **14** 1339–76

[186] Roet M, Hescham S-A, Jahanshahi A, Rutten B P, Anikeeva P O and Temel Y 2019 Progress in neuromodulation of the brain: A role for magnetic nanoparticles ? *Prog. Neurobiol.* **177** 1–14

[187] Kosari E and Vafai K 2020 Thermal tissue damage analysis for magnetothermal neuromodulation and lesion size minimization *Brain Multiphys.* **1** 100014

[188] Munshi R, Qadri S M, Zhang Q, Rubio I C, Del Pino P and Pralle A 2017 Magnetothermal genetic deep brain stimulation of motor behaviors in awake, freely moving mice *Elife* **6** e27069

[189] Chen R, Romero G, Christiansen M G, Mohr A and Anikeeva P 2015 Wireless magnetothermal deep brain stimulation *Science* **347** 1477–80

[190] Yang Y, Pacia C P, Ye D, Zhu L, Baek H, Yue Y, Yuan J, Miller M J, Cui J and Culver J P 2021 Sonothermogenetics for noninvasive and cell-type specific deep brain neuromodulation *Brain Stimulat.* **14** 790–800

[191] Bishnoi M, Bosgraaf C A, Aboojf U, Zhong L and Premkumar L S 2011 Streptozotocin-induced early thermal hyperalgesia is independent of glycemic state of rats: role of transient receptor potential vanilloid 1 (TRPV1) and inflammatory mediators *Mol. Pain* **7** 1744-8069-7–52

[192] Perigo E A, Hemery G, Sandre O, Ortega D, Garaio E, Plazaola F and Teran F J 2015 Fundamentals and advances in magnetic hyperthermia *Appl. Phys. Rev.* **2** 041302

[193] Salunkhe A B, Khot V M and Pawar S H 2014 Magnetic hyperthermia with magnetic nanoparticles: a status review *Curr. Top. Med. Chem.* **14** 572–94

[194] Bañobre-López M, Teijeiro A and Rivas J 2013 Magnetic nanoparticle-based hyperthermia for cancer treatment *Rep. Pract. Oncol. Radiother.* **18** 397–400

[195] Mahmoudi K, Bouras A, Bozec D, Ivkov R and Hadjipanayis C 2018 Magnetic hyperthermia therapy for the treatment of glioblastoma: a review of the therapy's history, efficacy and application in humans *Int. J. Hyperthermia* **34** 1316–28

[196] Wu K and Wang J-P 2017 Magnetic hyperthermia performance of magnetite nanoparticle assemblies under different driving fields *AIP Adv.* **7** 056327

[197] Munshi R 2019 *Magnetothermal Neuromodulation* (State University of New York at Buffalo) (https://www.proquest.com/docview/2194429258?pq-origsite=gscholar&fromopenview=true)

[198] Romero G, Christiansen M G, Stocche Barbosa L, Garcia F and Anikeeva P 2016 Localized excitation of neural activity via rapid magnetothermal drug release *Adv. Funct. Mater.* **26** 6471–8

[199] Loukin S, Zhou X, Su Z, Saimi Y and Kung C 2010 Wild-type and brachyolmia-causing mutant TRPV4 channels respond directly to stretch force *J. Biol. Chem.* **285** 27176–81

[200] Liedtke W, Choe Y, Martí-Renom M A, Bell A M, Denis C S, Hudspeth A J, Friedman J M and Heller S 2000 Vanilloid receptor–related osmotically activated channel (VR-OAC), a candidate vertebrate osmoreceptor *Cell* **103** 525–35

[201] Wheeler M A, Smith C J, Ottolini M, Barker B S, Purohit A M, Grippo R M, Gaykema R P, Spano A J, Beenhakker M P and Kucenas S 2016 Genetically targeted magnetic control of the nervous system *Nat. Neurosci.* **19** 756–61

[202] Tay A and Di Carlo D 2017 Magnetic nanoparticle-based mechanical stimulation for restoration of mechano-sensitive ion channel equilibrium in neural networks *Nano Lett.* **17** 886–92

[203] Coste B, Mathur J, Schmidt M, Earley T J, Ranade S, Petrus M J, Dubin A E and Patapoutian A 2010 Piezo1 and Piezo2 are essential components of distinct mechanically activated cation channels *Science* **330** 55–60

[204] Paoletti P and Ascher P 1994 Mechanosensitivity of NMDA receptors in cultured mouse central neurons *Neuron* **13** 645–55

[205] Wang P, Zhang E, Toledo D, Smith I T, Navarrete B, Furman N, Hernandez A F, Telusma M, McDaniel D and Liang P 2020 Colossal magnetoelectric effect in core–shell magnetoelectric nanoparticles *Nano Lett.* **20** 5765–72

[206] Kozielski K L, Jahanshahi A, Gilbert H B, Yu Y, Erin Ö, Francisco D, Alosaimi F, Temel Y and Sitti M 2021 Nonresonant powering of injectable nanoelectrodes enables wireless deep brain stimulation in freely moving mice *Sci. Adv.* **7** eabc4189

[207] Nguyen T, Gao J, Wang P, Nagesetti A, Andrews P, Masood S, Vriesman Z, Liang P, Khizroev S and Jin X 2021 *In vivo* wireless brain stimulation via non-invasive and targeted delivery of magnetoelectric nanoparticles *Neurotherapeutics* **18** 2091–106

[208] Singer A, Dutta S, Lewis E, Chen Z, Chen J C, Verma N, Avants B, Feldman A K, O'Malley J and Beierlein M 2020 Magnetoelectric materials for miniature, wireless neural stimulation at therapeutic frequencies *Neuron* **107** 631–43

[209] Galhardoni R, Correia G S, Araujo H, Yeng L T, Fernandes D T, Kaziyama H H, Marcolin M A, Bouhassira D, Teixeira M J and de Andrade D C 2015 Repetitive transcranial magnetic stimulation in chronic pain: a review of the literature *Arch. Phys. Med. Rehabil.* **96** S156–72

[210] Grossman E D, Battelli L and Pascual-Leone A 2005 Repetitive TMS over posterior STS disrupts perception of biological motion *Vision Res.* **45** 2847–53

[211] Aravinthan D, Sabareesan P and Daniel M 2015 Current induced magnetization switching in Co/Cu/Ni-Fe nanopillar with orange peel coupling *AIP Adv.* **5** 077166

[212] Levine D and Bockstahler B 2014 *Electrical Stimulation Canine Rehabilitation and Physical Therapy* (Philadelphia: Saunders) pp 342–58 (https://books.google.com/books?hl=en&lr=&id=ObIKAQAAQBAJ&oi=fnd&pg=PP1&dq=Levine+D+and+Bockstahler+B+2014+Electrical+stimulation+Canine+rehabilitation+and+physical+therapy+(Saunders,+Philadelphia)+pp+342%E2%80%9358&ots=586lrSQh5T&sig=b4C6ELQLUx2AWpzVQz725jM9HDo#v=onepage&q&f=false)

[213] Lake D A 1992 Neuromuscular electrical stimulation *Sports Med.* **13** 320–36

[214] Sluka K A and Walsh D 2003 Transcutaneous electrical nerve stimulation: basic science mechanisms and clinical effectiveness *J. Pain* **4** 109–21

[215] Chan M K, Tong R K and Chung K Y 2009 Bilateral upper limb training with functional electric stimulation in patients with chronic stroke *Neurorehabil. Neural Repair* **23** 357–65

[216] Tan A J, Huang M, Avci C O, Büttner F, Mann M, Hu W, Mazzoli C, Wilkins S, Tuller H L and Beach G S 2019 Magneto-ionic control of magnetism using a solid-state proton pump *Nat. Mater.* **18** 35

[217] Bauer U, Yao L, Tan A J, Agrawal P, Emori S, Tuller H L, Van Dijken S and Beach G S 2015 Magneto-ionic control of interfacial magnetism *Nat. Mater.* **14** 174–81

[218] Duschek K, Pohl D, Fähler S, Nielsch K and Leistner K 2016 Research Update: Magnetoionic control of magnetization and anisotropy in layered oxide/metal heterostructures *APL Mater.* **4** 032301

[219] Wang J-P and Saha R Magnetoionic controlled magnetism: Spintronic nanodevice for low power, cellular-level, magnetic neurostimulation PCT Application No. PCT/US2021/025313